Neurobiology of Disease

Dysregulation of NAD$^+$ Metabolism Induces a Schwann Cell Dedifferentiation Program

Yo Sasaki,* Amber R. Hackett,* Sungsu Kim, Amy Strickland, and Jeffrey Milbrandt
Department of Genetics, Washington University School of Medicine, St. Louis, Missouri 63110

The Schwann cell (SC) is the major component of the peripheral nervous system (PNS) that provides metabolic and functional support for peripheral axons. The emerging roles of SC mitochondrial function for PNS development and axonal stability indicate the importance of SC metabolism in nerve function and in peripheral neuropathies associated with metabolic disorders. Nicotinamide adenine dinucleotide (NAD$^+$) is a crucial molecule in the regulation of cellular metabolism and redox homeostasis. Here, we investigated the roles of NAD$^+$ metabolism in SC functions *in vivo* by mutating NAMPT, the rate-limiting enzyme of NAD$^+$ biosynthesis, specifically in SCs. NAMPT SC knock-out male and female mice (NAMPT SCKO mice) had delayed SC maturation in development and developed hypomyelinating peripheral neuropathy without axon degeneration or decreased SC survival. JUN, a master regulator of SC dedifferentiation, is elevated in NAMPT SCKO SCs, suggesting that decreased NAD$^+$ levels cause them to arrest at an immature stage. Nicotinic acid administration rescues the NAD$^+$ decline and reverses the SC maturation defect and the development of peripheral neuropathy, indicating the central role of NAD$^+$ in PNS development. Upon nicotinic acid withdrawal in adulthood, NAMPT SCKO mice showed rapid and severe peripheral neuropathy and activation of ERK/MEK/JUN signaling, which in turn promotes SC dedifferentiation. These data demonstrate the importance of NAD$^+$ metabolism in SC maturation and nerve development and maintenance and suggest that altered SC NAD$^+$ metabolism could underlie neuropathies associated with diabetes and aging.

Key words: metabolism; myelin; NAD$^+$; NAMPT; peripheral neuropathy; Schwann cell

Significance Statement

In this study, we showed that Schwann cell differentiation status is critically dependent on NAD$^+$ homeostasis. Aberrant regulation of NAD$^+$ biosynthesis via NAMPT deletion results in a blockade of Schwann cell maturation during development and severe peripheral neuropathy without significant axon loss. The phenotype can be rescued by supplementation with nicotinic acid; however, withdrawal of nicotinic acid leads to Schwann cell dedifferentiation, myelination defects, and death. These results provide new therapeutic possibilities for peripheral neuropathies associated with NAD$^+$ decline during aging or diabetes.

Introduction

The sciatic nerve contains two types of axons: large-diameter myelinated axons and small nonmyelinated axons found in Remak bundles. Myelinated axons are wrapped by multiple layers of Schwann cell (SC) processes compacted into myelin. Each ~1 mm segment of axon is myelinated by a single SC. In contrast, multiple small-diameter axons are ensheathed by nonmyelinating SCs in Remak bundles where SC processes interdigitate between axons. In addition to insulating axons, recent reports have begun to describe the emerging role of SCs in the metabolic support of axons (Nave, 2010; Feldman et al., 2017). This hypothesis is supported by experimental models that disrupt metabolism in SCs. For example, mitochondrial dysfunction induced by depletion of COX10 or TFAM in SCs causes severe hypomyelination and axonal loss (Viader et al., 2011, 2013; Fünfschilling et al., 2012). Ablation of the central metabolic regulator LKB1 in SCs results in demyelination and small-fiber axon degeneration (Beirowski et al., 2014), and depletion of the metabolic/nutrient sens-

Received Nov. 3, 2017; revised May 21, 2018; accepted June 12, 2018.

Author contributions: Y.S. and A.R.H. wrote the first draft of the paper; Y.S., A.R.H., and J.M. edited the paper; Y.S., A.R.H., and J.M. designed research; Y.S., A.R.H., S.K., and A.S. performed research; Y.S., A.R.H., A.S., and J.M. analyzed data; Y.S., A.R.H., and J.M. wrote the paper.

This work was supported by the National Institutes of Health Grants R56NS099314 and R01AG013730 to J.M., Grant T32NS007205 to A.R.H., and Grant R01NS087632 to J.M. and Aaron DiAntonio, Foundation for Barnes Jewish Hospital Cancer Frontier Fund and Siteman Cancer Center Grant to Aaron DiAntonio and J.M., and Hope Center Viral Vectors Core at Washington University School of Medicine. We thank Viviana Gradinaru and Benjamin Deverman for the PHP.S plasmid; members of the J.M. laboratories; and Kimberly Kruse, Nina Panchenko, and Rachel McClarney for experimental assistance.

Y.S. and J.M. may derive benefits from licensing agreements with ChromaDex and Disarm Therapeutics, which provide any support for this work.

*Y.S. and A.R.H. contributed equally to this work.

Correspondence should be addressed to Dr. Yo Sasaki, Department of Genetics, Washington University School of Medicine, St. Louis, MO 63110. E-mail: sasaki@wustl.edu.

DOI:10.1523/JNEUROSCI.3304-17.2018
 0270-6474/18/386546-17$15.00/0

ing protein OGT results in progressive demyelination and axon loss (Kim et al., 2016). In these instances, abnormal SC metabolism leads to axon degeneration in addition to direct effects on SCs, suggesting that the effects of metabolic abnormalities associated with diabetes or aging could be exerted at the SC level.

Myelinating and nonmyelinating SCs in the adult sciatic nerve are originally derived from neural crest cells through two intermediate stages: SC precursors and immature SCs, which develop at E12-E13 and E13-E15, respectively, in mice (Jessen and Mirsky, 2005). This differentiation process is known to be controlled by multiple transcription factors, including SOX10, NFκB, SOX2, OCT6, YY1, NFATc4, NAB1/2, BRN2, and EGR2 (Krox-20) (Salzer, 2008, 2015). Remarkably, fully mature SCs in adult nerves are able to dedifferentiate into immature SCs after injury and provide essential support for nerve regeneration. Afterward, SCs once again differentiate into mature myelinating or nonmyelinating SCs to restore normal peripheral nerve function. Increased MEK and ERK signaling leading to increased JUN activity is a key step in SC reprogramming in response to nerve injury (Parkinson et al., 2008; Napoli et al., 2012; Cervellini et al., 2018). Interestingly, JUN also inhibits EGR2 (Krox-20) (Parkinson et al., 2008) leading to reduced expression of genes importation for myelination. However, the signals upstream of ERK/JUN after peripheral nervous system injury remain poorly understood.

The oxidized form of nicotinamide adenine dinucleotide (NAD$^+$) is an essential metabolite that regulates cellular redox and protein modifications mediated by SIRTs, PARPs, and ARTs (Imai and Guarente, 2014). Accordingly, NAMPT, the rate-limiting enzyme of NAD$^+$ biosynthesis, is an essential enzyme for various tissues. While homozygous knock-out of NAMPT is embryonic lethal, conditional knock-out of NAMPT in adult mice results in lethality within 10 d (Zhang et al., 2017). These mice display severe intestinal deficits, visceral fat depletion, and weight loss. Supporting its central role in cell physiology, cell type-specific deletion of NAMPT has revealed important functions for this enzyme in myocytes (Frederick et al., 2016), adipocytes (Stromsdorfer et al., 2016), neural progenitors (Stein and Imai, 2014), excitatory cortical neurons (Stein et al., 2014), and photoreceptor cells (Lin et al., 2016).

NAMPT synthesizes nicotinamide mononucleotide (NMN) from nicotinamide (Nam), and the NMN is converted to NAD$^+$ by NMNAT enzymes. NMN can also be produced from nicotinamide riboside (NR) by NRK enzymes. In addition, NAD$^+$ can be synthesized from nicotinic acid (NA). In this case, NAPRT synthesizes NA mononucleotide (NaMN) from NA and NaMN is converted to NA adenine dinucleotide (NaAD) by NMNAT enzymes. The NaAD is then converted to NAD$^+$ by NAD$^+$ synthetase. Among these pathways, NAMPT-mediated NAD$^+$ synthesis is the dominant pathway in mammalian cells (Nikiforov et al., 2015). In this study, we depleted NAMPT specifically in SCs to investigate the roles of NAD$^+$ metabolism in peripheral nerve functions.

Materials and Methods

Animals. All animal experiments were performed under the direction of institutional animal study guidelines at the Washington University in St. Louis. All mice were of pure C57BL/6 genetic background, and both male and female mice were used for all experiments. To generate mice with SC-specific deletion of NAMPT (referred to as NAMPT SCKO or KO), *MPZ-Cre*$^+$ (Feltri et al., 1999) mice were bred to *NAMPT*$^{F/F}$ mice in which NAMPT exons 5 and 6 are flanked by loxP sites (Rongvaux et al., 2008). NA (Sigma-Aldrich) was diluted to 300 mg/dl in water (Lukasova et al., 2011) and provided to some groups of mice *ad libitum*. Littermate controls (referred to as WT) consisted of *NAMPT*$^{F/F}$*:MPZ-Cre*$^-$ mice and *NAMPT*$^{F/+}$*:MPZ-Cre*$^-$ mice.

Table 1. Antibodies

Antigen (species)	Catalog no.	Dilution
NAMPT (rabbit)	Bethyl A300-779A	Western (1:1000)
MBP (rat)	Millipore MAB386	Western (1:1000); IHC (1:500)
β-Actin (mouse)	Clone AC-74, Sigma-Aldrich A2228	Western (1:1000)
α-Rubulin (mouse)	Clone B-5-1-2, Sigma-Aldrich T5168	Western (1:1000)
Jun (rabbit)	Clone 60A8, Cell Signaling Technology #9165	Western (1:1000); IHC (1:300)
p-Mek (rabbit) Ser217/221	Clone 41G9, Cell Signaling Technology #9154	Western (1:1000)
p-ERK (rabbit) Thr202/Tyr204	Cell Signaling Technology #4370	Western (1:2000)
MPZ (chicken)	Aves PZO	Western (1:1000); IHC (1:500)
OCT6 (rabbit)	Abcam ab31766	Western (1:1000)
ERK (rabbit)	Cell Signaling Technology #4695	Western (1:2000)
CD68 (rat)	Bio-Rad MCA1957	IHC (1:500)
Neurofilament 200 (NF200) (rabbit)	Sigma-Aldrich N4142	IHC (1:500)
p75NTR (NGFR) (rabbit)	Clone D4B3, Cell Signaling Technology #8238	IHC (1:2000)

Table 2. qPCR primer sequences

Gene name	Forward sequence	Reverse sequence
NAMPT	GACTCGTACAAGGTTACTCAC	GTAGTTCCATCCTCTTTCGT
LGI4	GTGGATGCCTATGGTGAATGC	GCCGACTCCCCAACAGTCT
MBP	CCAGTAGTCCATTTCTTCAAGAACATT	AGCTAAATCTGCTGAGGGACAGG
EGR2	AGGCCCCTTTGACCAGATGA	AAGATGCCCGCACTCACAAT
BRN2	CAGCATAGACAAGATCGCAG	AAACCAAACTCTCACCACCT
EGR1	CAAACTGGAGGAGATGATGCTG	AAAGGACTCTGTGGTCAGGT
OCT6	CGCCAAGCAGTTCAAGCAA	TTGAGCAGCGGTTTGAGCTT
JUN	GAACTGCATAGCCAGAACAC	GTTGAAGTTGCTGAGGTTGG

Nerve electrophysiology. Compound muscle action potentials (CMAPs) were acquired as previously described (Beirowski et al., 2011) using a Viking Quest electromyography device (Nicolet). Mice were anesthetized; then electrodes (stimulating: ankle or sciatic notch; recording: footpad) were put into place. Supramaximal stimulation was used for CMAPs.

Western blot. Mice were anesthetized; then sciatic nerves segments were obtained, and the epineurium was removed in ice-cold PBS; then the nerves were frozen on dry ice and stored at −80°C. Sciatic nerves were sonicated in ice-cold lysis buffer (50 mM Tris-HCl, pH 7.5, 150 mM NaCl, 10 mM EDTA, 10 mM NaF, 0.1% SDS, 1% Triton X-100, 1% deoxycholate, 1% NP-40, and 100 mM PMSF with protease inhibitors, Roche Diagnostics; and phosphatase inhibitors, Sigma-Aldrich). Lysates were centrifuged at 12,000 × *g* for 20 min at 4°C, supernatant was collected, and 10–20 μg of protein was boiled for 5 min in sample buffer with β-mercaptoethanol, loaded onto 10% SDS-PAGE gels, and then transferred onto nitrocellulose membranes. Membranes were blocked in the blocking solution (Super Block T20, Thermo Fisher Scientific) and then incubated with antibodies (Table 1) diluted in blocking solution. Membranes were washed, incubated in species-appropriate secondary antibodies (Cell Signaling Technology), and then developed using Western Bright Quantum (Advansta). Band intensity was measured using ImageJ (National Institutes of Health), normalized to β-actin or α-tubulin, and then displayed as fold change relative to the average of the WT samples.

qPCR. Sciatic nerves were homogenized in Trizol (Thermo Fisher Scientific); then RNA was extracted as described in the protocol. RNA was reverse-transcribed using Quanta qScript (Quantabio), and then qPCR was performed using SYBR Green Master Mix (Quantabio) in a QuantStudio 3 Real-Time PCR Machine (ABI). C_t values were obtained, normalized to GAPDH, and then fold changes were calculated using the $\Delta\Delta C_t$ method. Primers sequences are displayed in Table 2.

Nerve structural analysis using light and electron microscopy. Sciatic nerves were processed as previously described (Geisler et al., 2016). Nerves were fixed in 3% glutaraldehyde in 0.1 M PBS (Polysciences)

overnight at 4°C, washed, then stained with 1% osmium tetroxide (Sigma-Aldrich) overnight at 4°C. Nerves were then washed, dehydrated in a serial gradient of ethanol from 50% to 100%. After dehydration, nerves were incubated in 50% propylene oxide/50% ethanol, then 100% propylene oxide. Subsequently, nerves were incubated in the Araldite resin solution/propylene oxide solutions overnight in the following ratios: 50:50, 70:30, 90:10, and then finally embedded in 100% Araldite resin solution (Araldite: DDSA: DMP30; 12:9:1; Electron Microscopy Sciences) and then baked overnight at 60°C. For the light microscope analysis, semithin sections of 400–600 nm were then cut using Leica EM UC7 Ultramicrotome and placed onto microscopy slides. For the electron microscopy study, 300–400 nm sections were collected onto copper grids and then stained with uranyl acetate and lead citrate and imaged with transmission electron microscopy (JEOL1200).

Axon labeling using adeno-associated virus (AAV). A modified AAV virus was generated by transfecting HEK293T cells with the PHP.s (Chan et al., 2017) capsid plasmid together with pAAV-hSyn-GFP and a helper plasmid. The cell medium was collected 72 h later, and virus was purified using the iodixanol gradient method. All viral preparation was performed by the Hope Center Viral Vectors Core. The PHP.s plasmid was provided under a Material Transfer Agreement. pAAV-hSyn-EGFP was a gift from Bryan Roth (Addgene, plasmid #50465). The viral supernatant (20 μl) was injected into the intrathecal space of P10 mouse pups. At age P35, mice were anesthetized and then transcardially perfused with 20 ml PBS followed by 4% PFA in PBS. Whole spinal columns were dissected out and postfixed in 4% PFA in PBS overnight. The following day, dorsal roots were dissected from the lumbar spinal cord, washed with PBS, and then whole-mounted on slides with Vectashield. Three random fields were imaged on a DMI 4000B confocal microscope (Leica Microsystems) using a 40× oil objective and a DFC 7000-T camera (Leica Microsystems) for each animal. Three-dimensional reconstructions were made using Bitplane Imaris. The quantification of dilated axons was done by using ImageJ (National Institutes of Health). The dilated structures (size of 13–130 μm^2) of axons with higher fluorescence intensity (>20% of maximum fluorescent intensity) in the confocal dorsal root images were detected by a particle analyzer tool. The total axon area was determined by the total number of fluorescently positive pixels. The content of dystrophic neurites was expressed as a percentage of area occupied by dilated axons over total axons.

Toluidine blue staining and quantification. Slides were stained with 1% toluidine blue solution (1% toluidine blue, 2% borax), washed with acetone and xylene, and then mounted in Cytoseal XTL (Thermo Fisher Scientific). Whole nerves were imaged at 20× magnification, and 3 random fields were obtained using a 100× oil-immersion lens. All myelinated axons were blindly counted per field, normalized to axons per square millimeter, and then averaged between the 3 fields. Axons that were demyelinated or showed myelin splitting, myelin infolding/outfolding, or axon degeneration were considered aberrant axons. To determine G-ratio, 100× images were cropped into random fields, and axon and fiber diameters for 120 axons per genotype (40 axons per mouse) were calculated using ImageJ.

Immunohistochemistry. Sciatic nerves were fixed in 4% PFA in PBS for 1 h at room temperature and then placed in 30% sucrose in PBS overnight at 4°C. Nerves were then embedded in OCT (Tissue-Tek), frozen on dry ice, and then stored at −80°C. Longitudinal sections of 6 μm or cross-sections of 20 μm were obtained using a cryostat and slides were stored at −20°C. Slides were fixed in cold acetone, washed with PBS, blocked with 5% normal goat serum in PBS with 0.3% Triton X-100, and incubated in primary antibodies (Table 1) overnight with blocking buffer. Slides were then washed, incubated in species appropriate secondary antibodies (Jackson ImmunoResearch Laboratories), washed, and then mounted in Vectashield with DAPI. Three random fields were imaged per nerve for each animal using a DMI 4000B confocal microscope (Leica Microsystems) with a 20× oil objective and DFC 7000-T camera (Leica Microsystems).

TUNEL apoptosis detection. TUNEL was performed as previously described with some modifications (Gavrieli et al., 1992; Hackett et al., 2016). Slides prepared for immunohistochemistry were thawed then postfixed with 4% PFA for 10 min at room temperature, washed thoroughly with PBS, incubated with 10 μg/ml proteinase K for 15 min at 37°C, then washed with PBS. A positive control slide was incubated in DNase I (1 U/ml) for 1 h at 37°C, then washed with PBS. Slides were then pretreated with TdT buffer (25 mM Tris-HCl, 200 mM sodium cacodylate, 0.25 mg/ml BSA, 1 mM cobalt chloride, Roche Diagnostics) at 37°C for 10 min. To perform end-labeling, TdT buffer was combined with terminal deoxynucleotidyl transferase (Roche Diagnostics, 400 U/slide) and Biotin-16-dUTP (Roche Diagnostics, 4 μM) and added to slides for 1 h at 37°C. Slides were thoroughly washed with PBS, then blocked for 30 min with 5% normal goat serum in PBS with 0.3% Triton-X, then incubated with Alexa-Fluor-conjugated streptavidin (Jackson ImmunoResearch Laboratories) for 30 min at 37°C. Slides were washed, and then mounted in Vectashield with DAPI. Three random fields were taken per nerve using a DMI 4000B confocal microscope (Leica Microsystems) using a 20× objective and a DFC 7000-T camera (Leica Microsystems). The total number of TUNEL$^+$ and DAPI$^+$ cells were quantified, normalized to tissue area, and then averaged. All TUNEL$^+$ cells were DAPI$^+$. In the positive control slides (DNase-treated), all DAPI$^+$ nuclei were TUNEL$^+$.

Mass spectroscopy. Mice were anesthetized; then sciatic nerves segments were obtained, the epineurium was removed in ice-cold PBS, and then the nerves were frozen on dry ice and stored at −80°C. Metabolites were extracted by homogenizing frozen sciatic nerves in 50% MeOH (100 μl per nerve) using sonication and incubated 10 min on ice. The homogenates were centrifuged (10,000 × *g* for 15 min), and the supernatants containing small metabolites and the precipitates containing proteins were collected. The metabolite-containing fractions were further purified with chloroform (50 μl) extraction. The precipitates containing proteins were solubilized by adding 0.1% SDS solution (100 μl per nerve), and the protein content was determined using BCA protein assay kit (Thermo Fisher Scientific). The aqueous phase (90 μl) was lyophilized and stored at −20°C until analysis. Lyophilized samples were reconstituted with 15 μl of 5 mM ammonium formate.

For SC metabolite assays, mouse SCs were cultured in 24 well plates (Ratner et al., 2006). Briefly, E12.5 mouse DRG were enzymatically dissociated in 0.25% trypsin, and then cultured in Neurobasal-containing 100 ng/ml NGF (Harlan) and 2% B27 (Invitrogen) in uncoated plastic dishes. A week later, SC-axon networks were removed from the plate and trypsinized. Isolated SCs were expanded in Neurobasal, B27, 5% FBS culture media in PDL-coated plates. Cells were then washed with 0.9% NaCl, and then metabolites were extracted with 50% MeOH (160 μl per well). Metabolite-containing solutions were transferred to microcentrifuge tube, mixed with 50 μl chloroform, and then centrifuged (12,000 × *g* for 15 min). The aqueous phase, which contained the metabolites (140 μl), was lyophilized and then reconstituted with 15 μl of 5 mM ammonium formate. To measure total protein, cells left on the plate were homogenized in 0.1% SDS (100 μl), and protein content was determined using a BCA protein assay kit (Thermo Fisher Scientific). FK866 was obtained from National Institute of Mental Health Chemical Synthesis and Drug Supply Program (MH #F-901).

Samples and standard compounds (ATP, NAD$^+$, NMN, NaAD) were injected into reverse phase column (Atlantis T3, 2.1 × 150 mm, 3 μm; Waters) at a flow rate of 0.15 ml/min with 5 mM ammonium formate for mobile phase A and 100% methanol for mobile phase B (B). Metabolites were eluted with gradients of 0%–70% of B from 0 to 10 min, 70% B from 10 to 15 min, 0% B from 16 to 20 min, using HPLC (1290, Agilent Technologies). The metabolites were detected with a Triple Quad mass spectrometer (6470 MassHunter; Agilent Technologies) under positive ESI multiple reaction monitoring. Metabolites were quantified by the MassHunter quantitative analysis tool (Agilent Technologies) with standard curves.

Alternative metabolite analysis targeting metabolites in the glycolysis pathway was performed as instructed (Metabolomics dMRM Database and Method, Agilent Technologies). Metabolites were extracted as described above and chromatographically separated using a reverse phase column (Zorbax RRHD Extend-C18, 2.1 × 150 mm, 1.8 μm, Agilent Technologies) with mobile buffer A (3% MeOH, 10 mM tributylamine, 15 mM acetic acid) and 0%–99% gradient of buffer B (100% MeOH, 10 mM tributylamine, 15 mM acetic acid). Metabolites were analyzed by mass spectrometer (6470, Agilent Technologies) using dynamic multiple

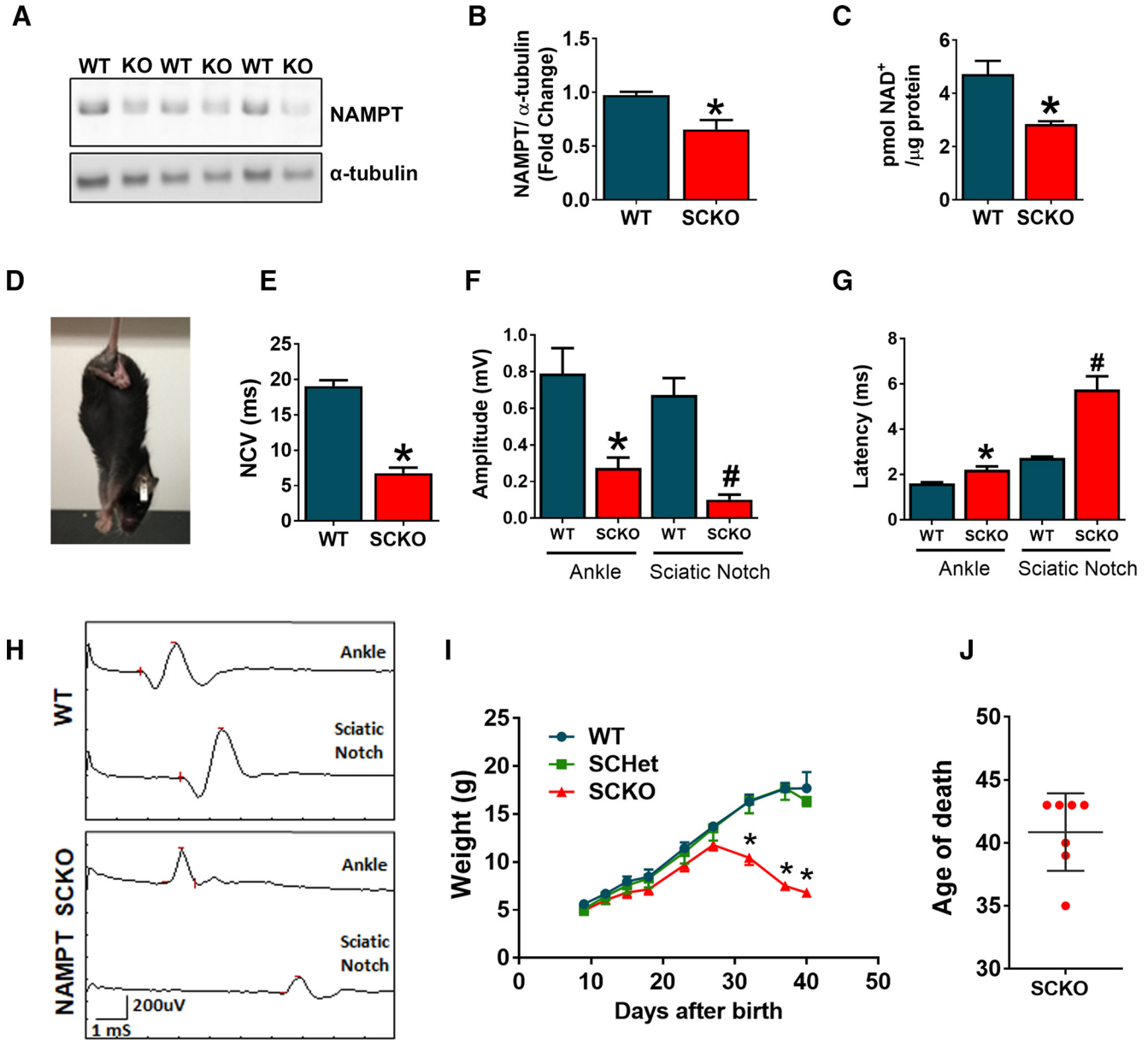

Figure 1. SC-specific deletion of NAMPT leads to severe neuropathy. ***A***, Western blot analysis of NAMPT expression and (***B***) quantification of fold change of NAMPT protein (normalized to α-tubulin) in sciatic nerves of P21 WT and NAMPT SCKO mice. $^*p = 0.0264$, unpaired two-tailed Student's *t* test ($n = 3$ mice). ***C***, NAD$^+$ levels (pmol) normalized to protein levels in sciatic nerves from P28 WT and NAMPT SCKO mice were determined by LC-MS/MS. $^*p < 0.01$, unpaired two-tailed Student's *t* test ($n = 4$ mice). ***D***, Characteristic hindlimb clasping in a NAMPT SCKO mouse at 1 month of age. ***E***, Nerve conduction velocity of WT and NAMPT SCKO mice at 35 d of age. $^*p < 0.0001$, unpaired two-tailed Student's *t* test ($n = 6$ or 7 mice). ***F***, Quantification of CMAP peak amplitude after ankle and sciatic notch stimulation of WT and NAMPT SCKO mice. $^*p = 0.008$, compared with WT at the ankle. $^\#p = 0.002$, compared with WT at the sciatic notch using unpaired two-tailed Student's *t* test ($n = 6$ or 7 mice). ***G***, Quantification of CMAP latency period after ankle and sciatic notch stimulation of WT and NAMPT SCKO mice. $^*p = 0.002$, compared with WT at the ankle. $^\#p = 0.0002$, compared with WT at the sciatic notch using unpaired two-tailed Student's *t* test ($n = 6$ or 7 mice). ***H***, Sample traces of CMAP recordings from the ankle and the sciatic notch in WT and NAMPT SCKO mice. Scale shown on the bottom left. ***I***, Growth curves of WT and NAMPT SCKO mice showing weight loss beginning at 1 month of age. Two-way ANOVA ($F_{(8,94)} = 91.2$, $p < 0.0001$ for time; $F_{(8,94)} = 91.2$, $p < 0.0001$ for genotype; $F_{(2,94)} = 79.34$, $p < 0.0001$ for interaction). $^*p < 0.0001$, multiple comparisons with Tukey's *post hoc* test ($n = 4 – 6$ mice). ***J***, NAMPT SCKO mice die ~40 d of age. Data are mean ± SEM.

reaction monitoring. The compound signatures, including retention time and qualifying ions, are predetermined in the dynamic multiple reaction monitoring database and data analysis tool automatically detect these compounds. After filtering out low abundance metabolites (area under curve <200), the relative amount of each metabolites was calculated and normalized by the amount of protein.

SC culture and in vitro *differentiation.* Primary rat SCs were cultured from rat P1 sciatic nerves as previously described (Nagarajan et al., 2001). For SC *in vitro* differentiation assays, SCs were initially seeded onto collagen-coated 24-well plates (100,000 cells/well) in 10% FBS-DMEM media supplemented with 2 μM forskolin and 20 μg/ml of bovine pituitary extract. After 72 h, the medium was switched to 1% FBS-DMEM media for 2 d, and then either DMSO or FK866 (100 nM) was added with or without NMN (Sigma-Aldrich, 100 μM). For SC differentiation, the cell-permeable cAMP analog 8-CPT-cAMP (Biolog, 250 μM) was added 16 h after FK/NMN addition, and RNA was collected 36 h after 8-CPT-cAMP addition using Trizol (Thermo Fisher Scientific). qPCR was performed as described in qPCR.

Experimental design and statistical analysis. Sample number (n) was defined as the number of animals that were independently manipulated and measured. No statistical evaluations were performed to predetermine sample sizes, but our sample sizes are similar to those generally used in the field. Generally, histology, Western, and qPCR assays were performed in 3 or 4 mice, whereas behavior and electrophysiology tests were

Movie 1. NAMPT SCKO mouse at 1 month of age. This mouse showed hindlimb paralysis and gait defects.

performed with >5 animals per cohort because there is more inherent variability between individual animals in these types of tests. Male and female animals were used in all experiments. Statistics were performed using Prism (GraphPad).

Results

NAMPT SCKO mice develop a severe peripheral neuropathy

NAMPT is the rate-limiting enzyme of NAD^+ biosynthesis and plays pivotal roles in cellular metabolism. Recent studies suggest the importance of SC metabolism in peripheral nerve development and homeostasis (Viader et al., 2011; Beirowski et al., 2014; Feldman et al., 2017). To further understand the role of SC metabolism in peripheral nerve function, we decided to manipulate SC NAD^+ metabolism by depleting NAMPT specifically in SCs (NAMPT-SCKO). NAMPT SCKO was generated by mating mice with a floxed NAMPT allele (Rongvaux et al., 2008) to mice expressing Cre recombinase under control of the MPZ promoter (Feltri et al., 1999). These mice express Cre in SCs beginning at E14, thus enabling gene deletion early in development. We confirmed that NAMPT protein levels were reduced in sciatic nerves from NAMPT SCKO mice by Western blotting (Fig. 1*A*,*B*). Consistent with the loss of NAMPT, NAD^+ levels were reduced in NAMPT SCKO nerves at postnatal days 28 (P28) when compared with those from WT (Fig. 1*C*). NAMPT SCKO mice displayed characteristics of peripheral neuropathy, such as hindlimb clasping (Fig. 1*D*), and gait abnormalities (Movie 1) at ~1 month of age. Consistent with these observations, CMAPs showed a severe loss in conduction velocity (Fig. 1*E*), decline in peak amplitude (Fig. 1*F*,*H*), and an increase in latency (Fig. 1*G*,*H*). Surprisingly, these mice started to lose weight ~P25 and died ~2 weeks later (~P40) (Fig. 1*I*,*J*). Together, these results show that NAMPT loss in SCs causes a reduction in NAD^+ levels and severe peripheral neuropathy.

NAMPT SCKO mice have severe defects in radial sorting and myelination

To investigate the cause of the severe peripheral neuropathy in NAMPT SCKO mice, we studied the structure of WT and NAMPT SCKO sciatic nerves in P0, P14, and P35 animals. Consistent with the electrophysiology data, NAMPT SCKO mice had significantly fewer myelinated axons at P14 and P35 (Fig. 2*A*–*C*). In the myelinated axons that were present, the G-ratio was significantly increased, indicating a reduction in myelin thickness, especially in larger-diameter axons (Fig. 2*D*,*E*). In addition, there were clear defects in the structure of Remak bundles in the NAMPT SCKO sciatic nerve at P14, as highlighted by the presence of large-diameter axons (>1 μm) that are normally sorted out of the Remak bundle by this age, and by a lack of SC process interdigitation among axons (Fig. 2*F*). These results suggest that P14 NAMPT SCKO mice have an early-stage radial sorting defect (delayed at Stage 1) (Feltri et al., 2015). By P35, most large-diameter axons in the NAMPT SCKO sciatic nerve have established a one-to-one relationship with SCs (Fig. 2*A*); however, the Remak bundles show a lack of SC process interdigitation between axons (Fig. 2*F*) and frequently contain large-diameter axons, suggesting that radial sorting remains arrested at Stage 4/5 (Feltri et al., 2015). These results suggest that hypomyelination and delayed radial sorting underlie the peripheral neuropathy in NAMPT SCKO mice.

To determine whether the reduction of properly myelinated axons and delayed axonal sorting are due to a lack of proliferation of SC progenitors, we counted the number of SC nuclei in P0 sciatic nerves (Fig. 2*G*,*H*). There were no significant differences in the number of SC nuclei, suggesting that the defects arise from their failure to sort axons properly and initiate (or complete) myelination. The number of SC nuclei in WT and NAMPT SCKO nerves were also similar at P14 and P35 (Fig. 2*I*,*J*), suggesting that SC death is not a factor in the abnormalities observed in the NAMPT SCKO nerves. To investigate further, we performed TUNEL staining in P35 WT and NAMPT SCKO mice. While WT sciatic nerve showed no $TUNEL^+$ cells, a small number were $TUNEL^+$ (5.97 ± 2.73 cells/mm^2, 0.8% of cells) in P35 NAMPT SCKO. These changes did not lead to a significant decrease in the number of $DAPI^+$ nuclei at P35 (WT: 598 ± 49 cells/mm^2; SCKO: 796 ± 97 cells/mm^2). These data indicate that there is a minimal increase in SC death in NAMPT SCKO nerves. Overall, these results suggest that loss of NAMPT alters the SC maturation processes but does not significantly affect their proliferation or survival.

In an attempt to understand mechanisms underlying hypomyelination and radial sorting defects in NAMPT SCKO, we analyzed mRNA expression of a panel of genes related to SC development at P35 in these nerves. We found that genes associated with SC maturity, MBP, EGR2 (Krox-20), and LGI4 were downregulated, whereas genes whose expression is downregulated in mature nerves, BRN2, EGR1, and OCT6 were highly expressed (Fig. 3*A*,*B*). Interestingly, JUN, which is a major regulator of SC dedifferentiation, was dramatically upregulated in these mutant nerves. Consistent with the mRNA expression profiles, reduced protein levels of MBP (Fig. 3*C*,*D*), and elevated levels of OCT6 (Fig. 3*C*,*E*) and JUN (Fig. 3*F*,*G*) were observed. We confirmed that the majority of JUN expression was present in SCs and not in $CD68^+$ macrophages (Fig. 3*H*), suggesting that a dedifferentiation program is activated in the SCs of NAMPT SCKO mice. Supporting this notion, we saw increased expression of NGFR (p75), a marker of immature SCs, in NAMPT SCKO nerves (Fig. 3*I*). These data suggest that many SCs in NAMPT SCKO mice are either arrested before full maturation or subsequently dedifferentiate after maturation.

To further investigate the causal role of NAD^+ decline in SC differentiation, we used a SC *in vitro* differentiation assay. In this paradigm, the addition of cell-permeable cAMP analog 8-CPT-cAMP induces SCs to express the terminal differentiation marker

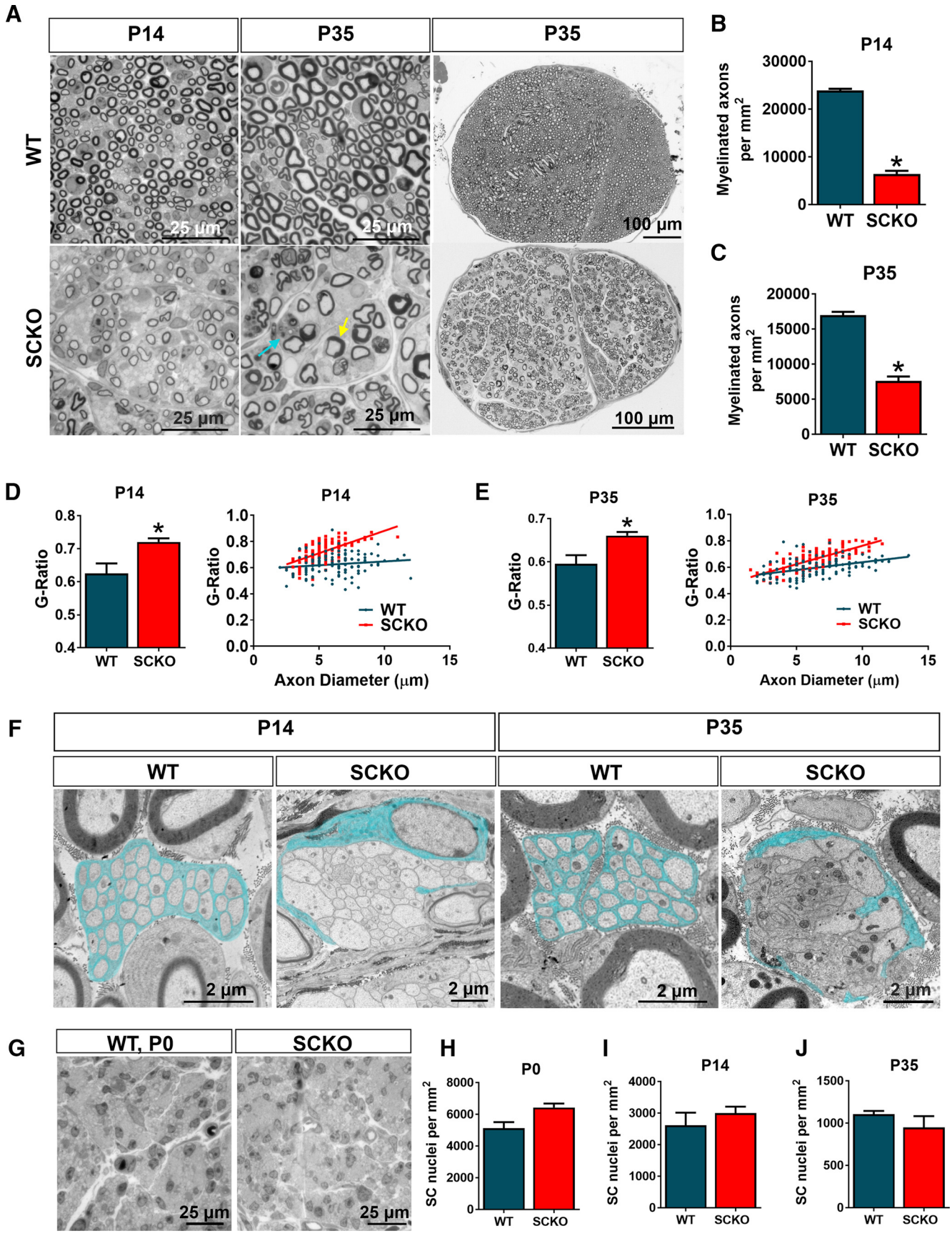

Figure 2. SC-specific deletion of NAMPT leads to improper SC development and myelination. ***A***, Representative images of toluidine blue-stained semithin cross-sections from sciatic nerves of WT and NAMPT SCKO mice at P14 or P35. Yellow arrow indicates aberrant myelin sheath. Blue arrow indicates a myelin-laden macrophage. Quantification of the number of myelinated axons per square millimeter at (***B***) P14 (*$p < 0.0001$, $n = 3$ mice) and (***C***) P35 ($p = 0.0003$, $n = 3$ mice) with unpaired two-tailed Student's *t* test in the sciatic nerves of WT and NAMPT SCKO mice. Average G-ratio and G-ratio versus axon diameter at (***D***) P14 ($p = 0.0427$, $n = 3$ mice) and (***E***) P35 ($p = 0.0398$, $n = 3$ mice) with unpaired two-tailed Student's *t* test. A total of (*Figure legend continues.*)

EGR2 (Krox-20) (Bacallao and Monje, 2015). We manipulated SC NAD$^+$ levels using a NAMPT-specific inhibitor FK866 (Hasmann and Schemainda, 2003). We observed a significant reduction of NAD$^+$ in these FK866-treated SCs, which could be rescued by the addition of NMN (an NAD$^+$ precursor downstream of NAMPT) (Fig. 3*J*). Consistent with previous reports, we observed a significant increase in EGR2 (Krox-20) expression after the application of CPT-cAMP (Fig. 3*K*). Importantly, CPT-cAMP induced EGR2 (Krox-20) expression was completely blocked by the presence of FK866 and was rescued by addition of NMN (Fig. 3*K*). These results strongly support the idea that the reduction of intracellular NAD$^+$ causes an inhibition of SC differentiation.

In addition to inadequate myelination, aberrantly myelinated fibers (Fig. 2*A*, yellow arrow) and naked axons were frequently observed in P35 NAMPT SCKO nerves (Fig. 4*A*, yellow arrows). Myelin-laden macrophages were also frequently observed (Figs. 2*A*, Fig. 4*A*, blue arrow) and the number of CD68$^+$ activated macrophages were greatly increased in P35 NAMPT SCKO nerves (Fig. 3*H*). These results suggest that the abnormalities caused by SC NAD$^+$ depletion leads to increased immune cell responses in NAMPT SCKO nerves.

Interestingly, we observed only minimal signs of axonal degeneration in NAMPT SCKO mice at all ages examined. Occasionally, degenerated axons, characterized by the presence of enlarged organelles, were observed (Fig. 4*A*, red arrow), but this was infrequent during the lifespan of NAMPT SCKO mice. To investigate this further, we stained sciatic nerves with neurofilament (NF200) and saw no obvious defects (data not shown). Because it is difficult to assess axon continuity in tissue sections, we decided to prelabel axons using AAV virus-expressing EGFP driven by the human Synapsin promoter (AAV-Syn-EGFP). We dissected dorsal roots from WT and NAMPT SCKO mice and prepared whole-mounted them on slides. We acquired confocal *z* stacks and could image >50 μm into the tissue, allowing us to view trajectories of axons after reconstruction using Bitplane Imaris. We occasionally observed dilated axons (Fig. 4*B*, white arrows). The percentage of area occupied by dilated axons over total axons was higher in NAMPT SCKO compared with WT: 0.50 ± 1.87% in NAMPT SCKO and 0.14 ± 0.33% in WT, $p = 0.003$, two-tailed unpaired Student's *t* test, $n = 323$ in WT ($n = 3$ mice) and 290 in NAMPT SCKO ($n = 3$ mice); however, the majority of axons remained intact in WT and NAMPT SCKO nerves. Thus, it is likely that the peripheral neuropathy in NAMPT SCKO is primarily due to the defects in radial sorting and myelination of axons by SCs rather than overt axon degeneration.

Because NAD$^+$ plays an important role in oxidative phosphorylation in the mitochondria, we hypothesized that there might be mitochondrial damage in NAMPT SCKO mice. In previous studies in which critical mitochondrial proteins were mutated in SCs, such as TFAM and COX10, the mitochondria were swollen and had diameters of >500 nm (Viader et al., 2011; Fünfschilling et al., 2012). We therefore made similar mitochondrial measurements in P35 NAMPT SCKO sciatic nerves to assess their mitochondria; however, no significant differences in SC mitochondrial density or diameter were observed (Fig. 4*E*,*F*). We did detect a modest increase in the density of mitochondria within the axons of these mutant nerves (Fig. 4*C*), while no difference in axonal mitochondria diameter was noted (Fig. 4*D*). Overall, NAMPT SCKO nerves did not show any overt damage to mitochondria.

Dietary supplementation with NA rescues the NAMPT SCKO peripheral nerve phenotype

NAD$^+$ levels decline in aged animals and in pathological conditions, such as diabetes (Yoshino et al., 2011; Verdin, 2015); thus, it is important to understand how NAD$^+$ levels affect nerve maintenance in adulthood. To this end, we used dietary supplementation in an attempt to rescue the developmental myelin defects in NAMPT SCKO. Although the major mammalian NAD$^+$ biosynthesis pathway uses Nam, the substrate of NAMPT, animals can also produce NAD$^+$ from NA using an alternative pathway involving the enzymes NAPRT, NMNAT, and NAD$^+$ synthetase (Fig. 5*A*). We administered NA (300 mg/dl) in the drinking water of the mothers during pregnancy and the perinatal period and directly to the progeny after weaning. Remarkably, not only did NA supplementation extend the lifespan of NAMPT SCKO mice (tested up to P62; Fig. 6*A*), it also resulted in sciatic nerves with grossly normal morphology (Fig. 5*B*) and restored myelination (Fig. 5*C*), CMAP responses (Fig. 5*D*), and nerve conduction velocities (Fig. 6*D*). Most NAMPT SCKO nerve abnormalities were completely reversed: the only exceptions were subtle changes in the G-ratio of larger-diameter axons (Fig. 5*C*) and radial sorting deficits (Fig. 5*E*). These results indicate that NAD$^+$ production using the alternative precursor NA was significant and sufficient to reverse the deficits caused by NAMPT loss.

Withdrawal of NA from adult NAMPT SCKO mice leads to rapidly progressive peripheral neuropathy

We next investigated whether the requirement for NAMPT in SCs was only critical during development or whether it was also necessary for nerve maintenance and proper function in adulthood. For this purpose, we acutely withdrew NA from P55 WT or NAMPT SCKO mice that had been maintained on this dietary supplement since conception (Fig. 6*A*). Interestingly, NAMPT SCKO mice lost ~4 g (~20%) of body weight and died within 7 d after NA withdrawal, whereas WT mice showed no abnormalities (Fig. 6*A*,*C*). After NA withdrawal, the NAMPT SCKO mice showed a gradual decline in nerve conduction velocity (Fig. 6*D*) and developed severe hindlimb paralysis (Fig. 6*B*; Movie 2). Overall, NA withdrawal in adulthood recapitulated the behavioral and neurological deficits observed during early development in untreated NAMPT SCKO mice (Fig. 1), indicating that maintaining NAD$^+$ levels in adulthood is critical for proper nerve function.

To understand the underlying mechanism of the neurological deficits observed in NAMPT SCKO mice after NA withdrawal, we analyzed myelin structures in the sciatic nerve using light and electron microscopy (Figs. 6, 7). In NAMPT SCKO mice, we observed fewer properly myelinated axons (Fig. 6*E*,*F*) and an increased number of aberrant fibers between 5 and 7 d after NA withdrawal (Fig. 6*E*,*G*) without altering SC numbers (Fig. 6*H*). These aberrant fibers had multiple types of abnormalities, including myelin infoldings (Fig. 7*A*, blue arrow), interlamellar myelin splitting (Fig. 7*A*, purple arrow), abnormal axo-glial junctions (Fig. 7*A*, orange arrow), and abnormal SC cytoplasm at the outer tongue (Fig. 7*A*, yellow arrows) that occasionally contained an increased number of mitochondria (Fig. 7*A*, red arrow). To fur-

←

(*Figure legend continued.*) 120 axons were quantified for mice ($n = 3$) of each genotype. ***F***, Electron microscopic images of a normal Remak bundle in WT sciatic nerve and unsorted bundled axons in P14 and P35 NAMPT SCKO mice. SC cytoplasm is pseudo-colored light blue. ***G***, Representative images of toluidine blue-stained semithin cross-sections of sciatic nerves from P0 WT and NAMPT SCKO mice. Quantification of the number of nuclei per square millimeter at (***H***) P0, (***I***) P14, and (***J***) P35 in the sciatic nerves of WT and NAMPT SCKO mice. ***I***, ***K***, Average G-ratio WT and NAMPT SCKO sciatic nerves at (***I***) P14 and (***K***) P35. ***H–J***, No significant difference with unpaired two-tailed Student's *t* test ($n = 3$ mice). Data are mean ± SEM.

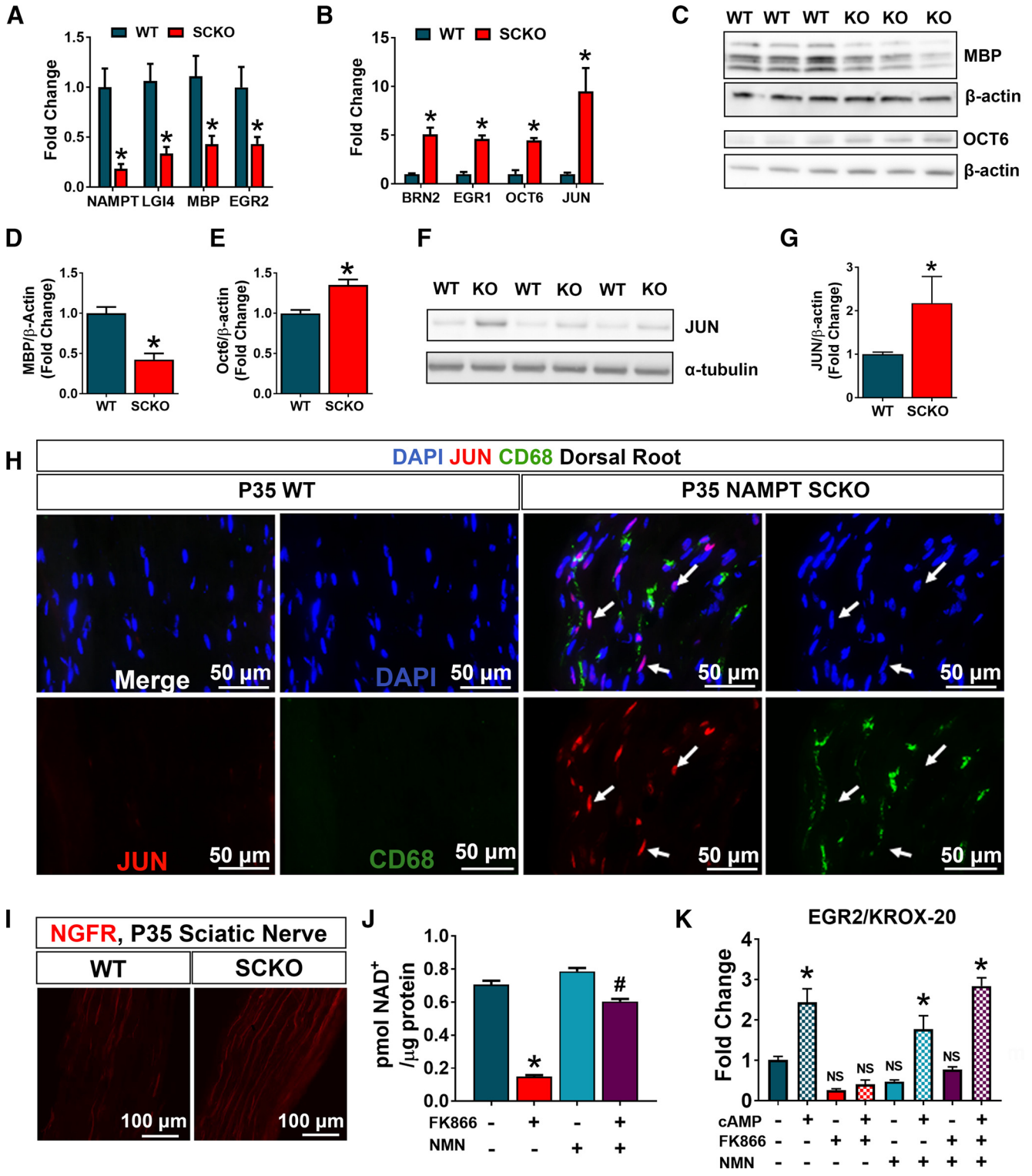

Figure 3. Markers of SC maturity are aberrantly regulated in NAMPT SCKO mice. ***A***, ***B***, qPCR analysis of mRNAs from sciatic nerves of WT and NAMPT SCKO mice at 35 d of age. Individual unpaired *t* tests for each gene with significance determined by the Sidak–Bonferroni method when $\alpha < 0.05$, $^*p < 0.03$ ($n = 3$–6). ***C***, ***F***, Western blot analysis and (***D***, ***E***, ***G***) quantification of fold change of (***C***, ***D***) MBP ($^*p < 0.0001$, $n = 3$) with Student's two-tailed *t* test, (***C***, ***E***) OCT6 ($^*p < 0.01$, $n = 3$) with Student's two-tailed *t* test, and (***F***, ***G***) JUN ($^*p < 0.007$, $n = 3$) with Student's two-tailed *t* test (normalized to β-actin or α-tubulin) in WT compared with NAMPT SCKO sciatic nerves at 1 month of age. ***H***, Immunostaining of nuclei (DAPI, blue), macrophages (CD68, green), and JUN (red) in longitudinal sections of dorsal roots of WT and NAMPT SCKO mice at P35. White arrows indicate Jun $^+$CD68 $^-$ cells. ***I***, Immunostaining of NGFR (p75) in WT and NAMPT SCKO sciatic nerves at 35 d of age. $n = 3$ or 4 mice. ***J***, NAD $^+$ levels were measured in primary SCs treated with vehicle (DMSO), 100 nM FK866, and/or 100 μM NMN for 24 h *in vitro*. One-way ANOVA with multiple comparisons: $F_{(3,12)} = 254$ ($n = 4$). $^*p < 0.0001$, compared with vehicle (DMSO). $^\#p < 0.0001$, compared with FK866 treatment alone by Tukey's *post hoc* test. ***K***, Primary SCs were treated with vehicle (DMSO) or 100 nM Fk866 with or without 100 μM NMN for 16 h before addition of 250 μM CPT-cAMP. Cells were harvested 3 h after addition of CPT-cAMP. NS, Not significant from vehicle SCs. $F_{(3,22)} = 28.38$ and $p < 0.0001$ for drug treatments, $F_{(1,22)} = 89.57$ and $p < 0.0001$ for CPT-cAMP treatment, $F_{(3,22)} = 9.577$ and $p = 0.0003$ for interaction ($n = 3$ or 4) using two-way ANOVA with multiple comparisons. $^*p < 0.001$, comparing treatments with or without CPT-cAMP for each combination of drug treatments (solid vs checkered bars of each color) using Tukey's *post hoc* test. Data are mean ± SEM.

ther assess mitochondria damage, we quantified the density and diameter of mitochondria in WT and NAMPT SCKO nerves, analyzing both SCs and axons at 0 versus 7 d after NA withdrawal. We saw no significant differences in these mitochondrial parameters (Fig. 7*B*,*C*), suggesting that mitochondrial damage is not a major contributor to the dramatic neurological phenotype of these mutant mice.

Similar to what we observed in P35 NAMPT SCKO nerves, we saw little cell death after NA withdrawal. At 5 d after NA withdrawal, only 1.8 ± 0.9 cells/mm^2 (0.5% of cells) were TUNEL$^+$. These changes did not lead to a significant decrease in the number of DAPI$^+$ nuclei at 5 d after NA withdrawal (WT: 486 ± 25 cells/mm^2; SCKO: 558 ± 31 cells/mm^2). Overall, these results suggest that SC death is not a major contributor to the phenotypes observed in NAMPT SCKO mice after NA withdrawal.

To assess axonal damage in NAMPT SCKO nerves after NA withdrawal, we initially quantified the density of nonmyelinated axons in WT and NAMPT SCKO nerves at 0, 5, and 7 d after NA withdrawal. We saw a modest decrease in axon density at 7 d after NA withdrawal (Fig. 7*D*), suggesting that nonmyelinated axonal integrity may be modestly compromised. To evaluate axonal integrity of large-diameter axons, sciatic nerves were stained with neurofilament NF200 (Fig. 7*E*). There were no obvious differences in NF200 distribution between WT and NAMPT SCKO sciatic nerves at 5 d after NA withdrawal, suggesting the absence of overt axonal degeneration.

Overall, these data strongly indicate that the neurological deficits occurring within days of NA withdrawal in NAMPT SCKO adult mice are due to aberrant SC-axon interactions and defective myelin maintenance. These studies point to the importance of maintaining adequate NAD$^+$ levels in SCs in adulthood and suggest that neuropathy in the elderly and in diabetics could be associated with the decrease in NAD$^+$ levels that occur in these conditions.

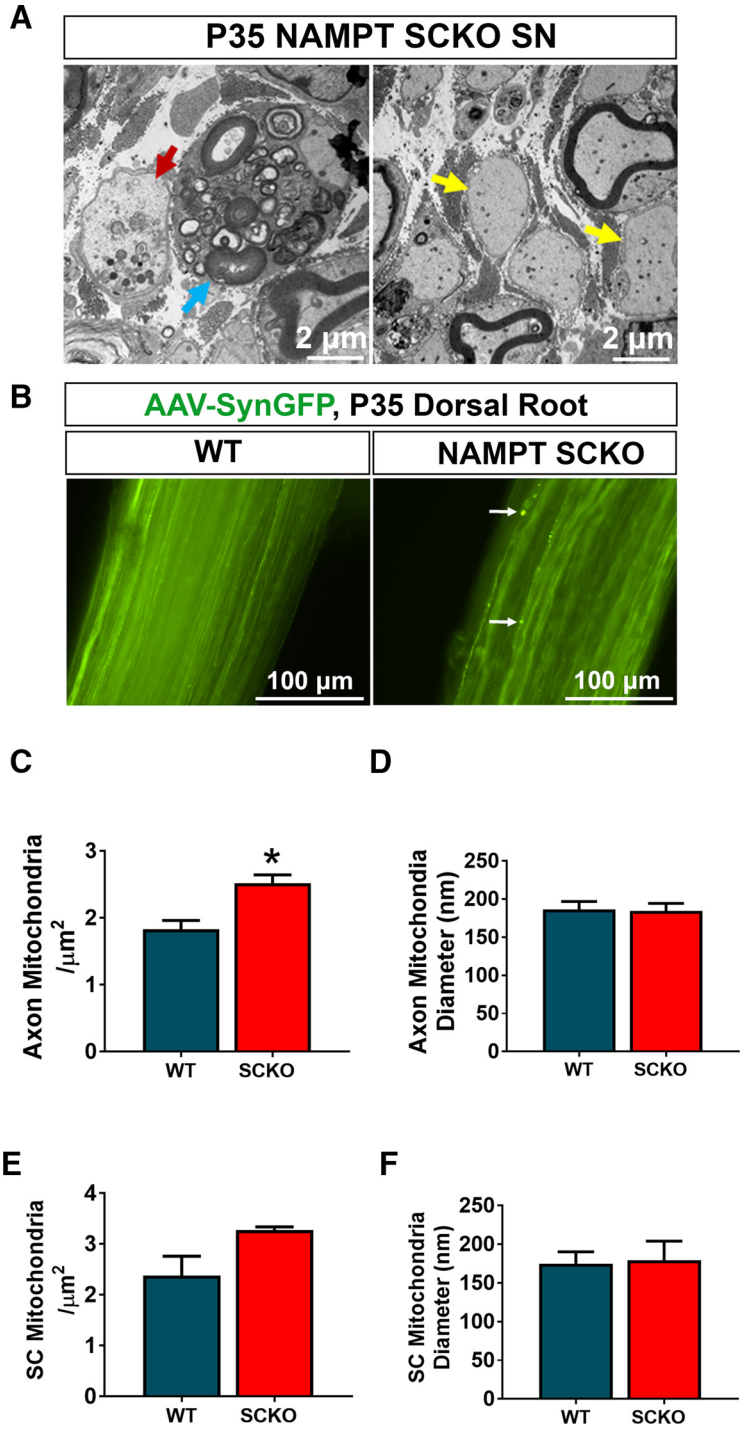

Figure 4. NAMPT SCKO does not induce severe axon degeneration. ***A***, Most axons in NAMPT SCKO mice do not show obvious signs of axon degeneration, but occasional fragmented axons were observed (red arrow). Naked axons (yellow arrows) and myelin-laden macrophages (blue arrow) were frequently observed in NAMPT SCKO nerves. ***B***, DRG neurons were infected with an AAV virus-expressing EGFP driven by the Synapsin promoter. Images shown are whole-mounted dorsal roots. While almost all axons were continuous, dilated axons were occasionally observed in NAMPT SCKO dorsal roots (white arrow). Mitochondria density (***C***, ***D***) and diameter (***E***, ***F***) were measured for both axons (***C***, ***D***) and SCs (***E***, ***F***) in P35 WT and NAMPT SCKO sciatic nerves using electron microscopic images. *$p = 0.02$ (unpaired two-tailed Student's t test). $n = 3$ mice for all experiments in this figure. Data are mean ± SEM.

Disruption of NAD$^+$ synthesis in adulthood yields major metabolic changes

To determine the metabolic consequences of NA administration, we performed metabolomics analysis using LC-MS/MS on sciatic nerves from WT and NAMPT SCKO mice that were administered NA from conception until death (0 d after NA withdrawal) or were killed 5 d after NA withdrawal. Because NAD$^+$ levels were comparable between NAMPT SCKO and WT mice after NA supplementation, we can conclude that NA is sufficient to rescue NAD$^+$ levels in NAMPT SCKO nerves (Fig. 8*A*). Withdrawal of NA resulted in the reduction of nerve NAD$^+$ levels both in WT and NAMPT SCKO due to an inactivation of NA-dependent NAD$^+$ synthesis. Five days after NA withdrawal, NAD$^+$ levels in NAMPT SCKO

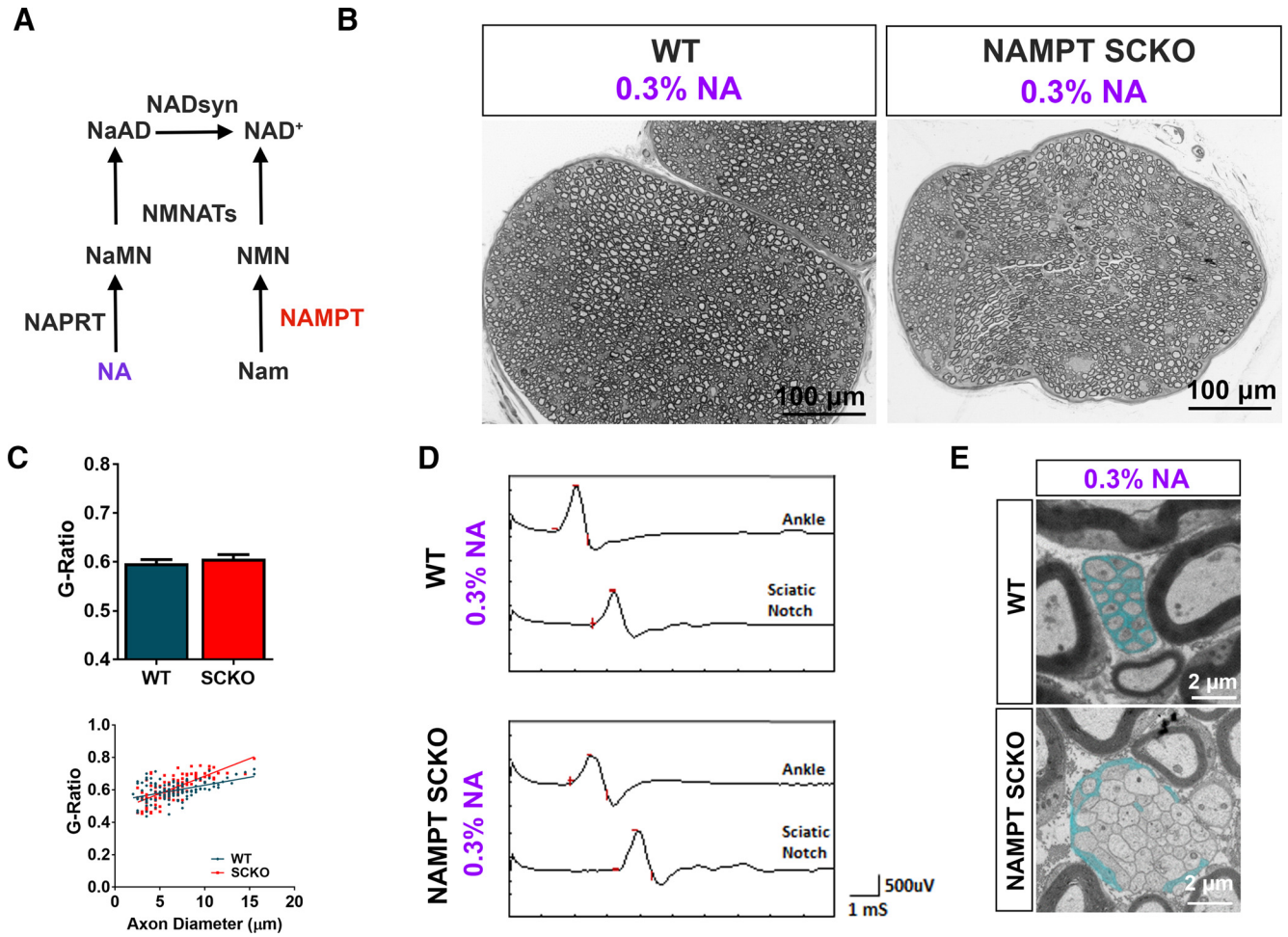

Figure 5. NA rescues developmental defects of NAMPT SCKO mice. ***A***, Diagram depicting NAD+ biosynthetic pathways. ***B***, Representative images of toluidine blue-stained semithin cross-sections from the sciatic nerves of WT and NAMPT SCKO mice at P62 that received 0.3% NA from conception until death. ***C***, Average G-ratio and G-ratio versus axon diameter for WT and NAMPT SCKO sciatic nerves after treatment with 0.3% NA. $n = 3$ animals with 120 axons quantified per genotype. Student's two-tailed t test yields no significant difference. ***D***, Sample traces of CMAP recordings from the ankle and sciatic notch stimulation of WT and NAMPT SCKO mice, which have received 0.3% NA. ***E***, Remak bundles in WT, but not NAMPT SCKO sciatic nerves, have SC process interdigitation between axons (SC cytoplasm is pseudo-colored light blue). NAMPT SCKO Remak bundles contained large-diameter axons compared with WT. $n = 3$ mice. Data are mean ± SEM.

nerves were significantly lower than WT because NAD+ is predominantly synthesized from Nam using NAMPT (Fig. 8*A*).

As expected, the levels of NaAD (a metabolic intermediate in NAD+ synthesis from NA) were significantly higher in animals supplemented with NA (Fig. 8*B*). Accordingly, NaAD levels declined to undetectable levels within 5 d after NA withdrawal in sciatic nerves from both WT and NAMPT SCKO mice (Fig. 8*B*). Interestingly, NMN levels correlated with NAD+, increasing upon NA administration and declining after NA withdrawal in both WT and NAMPT SCKO nerves (Fig. 8*C*). This indicates the existence of an efficient salvage pathway that breaks down NAD+ into Nam, and then reincorporates Nam into NMN via NAMPT present in the non-SC components of the nerve. Interestingly, ATP levels did not change in response to NA supplementation or depletion in WT or NAMPT SCKO nerves within the time frames examined (Fig. 8*D*). These results show that NA administration successfully restored nerve NAD+ levels in NAMPT SCKO mice and that this was sufficient to largely rescue the deficits associated with NAMPT loss.

Previous reports indicated that pharmacological inhibition or genetic ablation of NAMPT causes inhibition of glycolysis (Tolstikov et al., 2014; Tan et al., 2015; Frederick et al., 2016). This is presumably due to inhibition of GAPDH, an NAD+-dependent enzyme in the glycolytic pathway, as evidenced by accumulation of metabolites produced upstream of GAPDH (Fig. 8*E*). To investigate whether glycolysis is impaired in SCs lacking NAMPT, we used LC-MS/MS to measure glycolytic intermediates in sciatic nerves from WT and NAMPT SCKO mice that received NA supplementation up until death (day 0) or 5 d after NA withdrawal (day 5). We found a significant accumulation of glycolytic intermediates in the sciatic nerve of NAMPT SCKO, but not WT, mice in which NA had been withdrawn for 5 d (Fig. 8*E–H*,*J*, heat map). Metabolites that were increased included D-fructose 1,6-bisphosphate (Fig. 8*F*), dihydroxyacetone phosphate (Fig. 8*G*), and D-glyceraldehyde 3-phosphate (Fig. 8*H*). All of these metabolites precede the NAD+-dependent conversion of D-glyceraldehyde 3-phosphate into 1,3-bisphospho-D-glycerate by GAPDH (Fig. 8*E*), consistent with low GAPDH activity due to reduced NAD+ levels. In addition, pyruvate, the final product of glycolysis, was decreased in NAMPT SCKO nerves at 5 d after NA depletion compared with WT (Fig. 8*I*,*J*, heat map), indicating that glycolysis is inefficient in this situation.

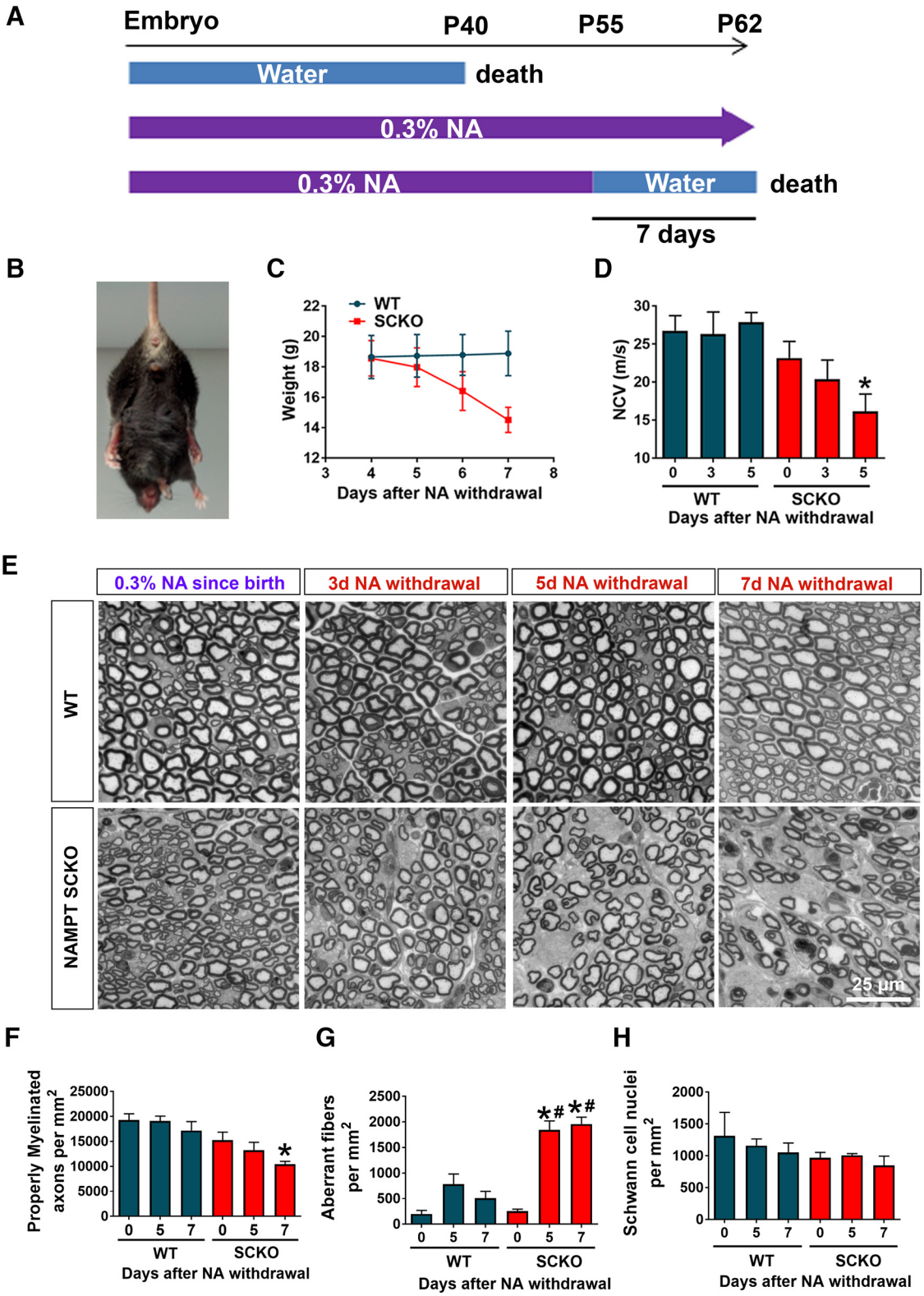

Figure 6. NA depletion in NAMPT SCKO mice results in severe neuropathy within days. ***A***, Schematic representation of NAMPT SCKO mice viability with or without NA treatment. ***B***, Characteristic hindlimb clasping in a NAMPT SCKO mouse 7 d after NA withdrawal. ***C***, Change in weight after NA withdrawal of WT and NAMPT SCKO mice. ***D***, Sciatic nerve conduction velocity from CMAP measurement decreases with time after NA withdrawal. One-way ANOVA ($F_{(5,26)} = 5.303, p = 0.0017$). *$p < 0.03$ ($n = 3$–9) with multiple comparisons with Sidak's *post hoc* test compared with WT with no NA withdrawal. ***D***, ***F–H***, One-way ANOVA with Sidak's *post hoc* test. ***E***, Representative images of toluidine blue-stained semithin cross-sections from the sciatic nerves of WT and NAMPT SCKO mice after NA withdrawal. ***F***, Quantification of the number of properly myelinated axons per square millimeter in WT and NAMPT SCKO mice after NA withdrawal. One-way ANOVA ($F_{(5,13)} = 5.621, p = 0.0056$). *$p = 0.0144$ ($n = 3$ mice) with multiple comparisons with Sidak's *post hoc* test compared with WT with no NA withdrawal. ***G***, Quantification of the number of aberrant fibers per square millimeter in WT and NAMPT SCKO mice after NA withdrawal. One-way ANOVA ($F_{(5,15)} = 29.16, p < 0.0001$). #$p < 0.0001$ ($n = 3$ mice) with multiple comparisons with Sidak's *post hoc* test compared with WT with no NA withdrawal. ***H***, Quantification of the number of SC nuclei per square millimeter in WT and NAMPT SCKO mice after NA withdrawal ($n = 3$ mice). No significant differences were found using one-way ANOVA. Data are mean ± SEM.

Movie 2. NAMPT SCKO or WT mouse at 55 d of age and 7 d after NA withdrawal. This NAMPT SCKO mouse showed severe hindlimb paralysis and gait defects.

Dysregulation of NAD$^+$ biosynthesis leads to upregulation of SC dedifferentiation pathways

The rapid progression of myelin abnormalities accompanying NAD$^+$ decline after NA withdrawal in NAMPT SCKO mice, coupled with the immature SC gene expression profile in these mutant mice perinatally (Fig. 3*B*,*E–I*), suggested that SC maturation is regulated by NAD$^+$ metabolism. This prompted us to examine the ERK/MEK signaling pathways that govern SC injury-induced dedifferentiation and redifferentiation (Napoli et al., 2012; Cervellini et al., 2018). We observed no changes in SC dedifferentiation pathways in NAMPT SCKO mice treated with NA (Fig. 9*A*), including phospho-MEK (Fig. 9*A*,*B*), phospho-ERK (Fig. 9*A*,*C*,*D*), and JUN (Fig. 9*A*,*E*). However, 3 d after NA withdrawal when NAD$^+$ levels had decreased, we observed upregulation of phospho-MEK (Fig. 9*F*,*G*), phospho-ERK (Fig. 9*F*,*H*), and JUN (Fig. 9*F*,*I*). These dedifferentiation hallmarks remained elevated 5 d after NA withdrawal (Fig. 9*J*,*K*,*M–O*). Additionally, we saw downregulation of MPZ (Fig. 9*L*,*P*) and MBP (Fig. 9*L*,*Q*), consistent with observations of the SC dedifferentiation program after nerve injury and, with the presence of myelin abnormalities after NA withdrawal in NAMPT SCKO mice (Fig. 7*A*). These results demonstrate that NA withdrawal and the subsequent changes in metabolism result in the activation of ERK/MEK/JUN signaling in nerves of NAMPT SCKO mice. Our results indicate that acute NAD$^+$ reduction in adult sciatic nerve activates signaling pathways associated with SC dedifferentiation despite the absence of nerve injury, a reaction that could lead to defective nerve maintenance and neuropathy in diseases with metabolic dysfunction.

Discussion

In this study, we investigated the effects of SC metabolic perturbation on peripheral nerve function by ablating NAMPT, the rate-limiting enzyme of NAD$^+$ synthesis, in SCs. NAMPT depletion in SCs during embryogenesis results in improper SC maturation, which in turn leads to radial sorting defects, hypomyelination, and hindlimb paralysis. We took advantage of the existence of an alternate, NAMPT-independent pathway for NAD$^+$ synthesis that uses NA and NAPRT to manipulate NAD$^+$ levels in NAMPT SCKO nerves. The adult NAMPT SCKO mice

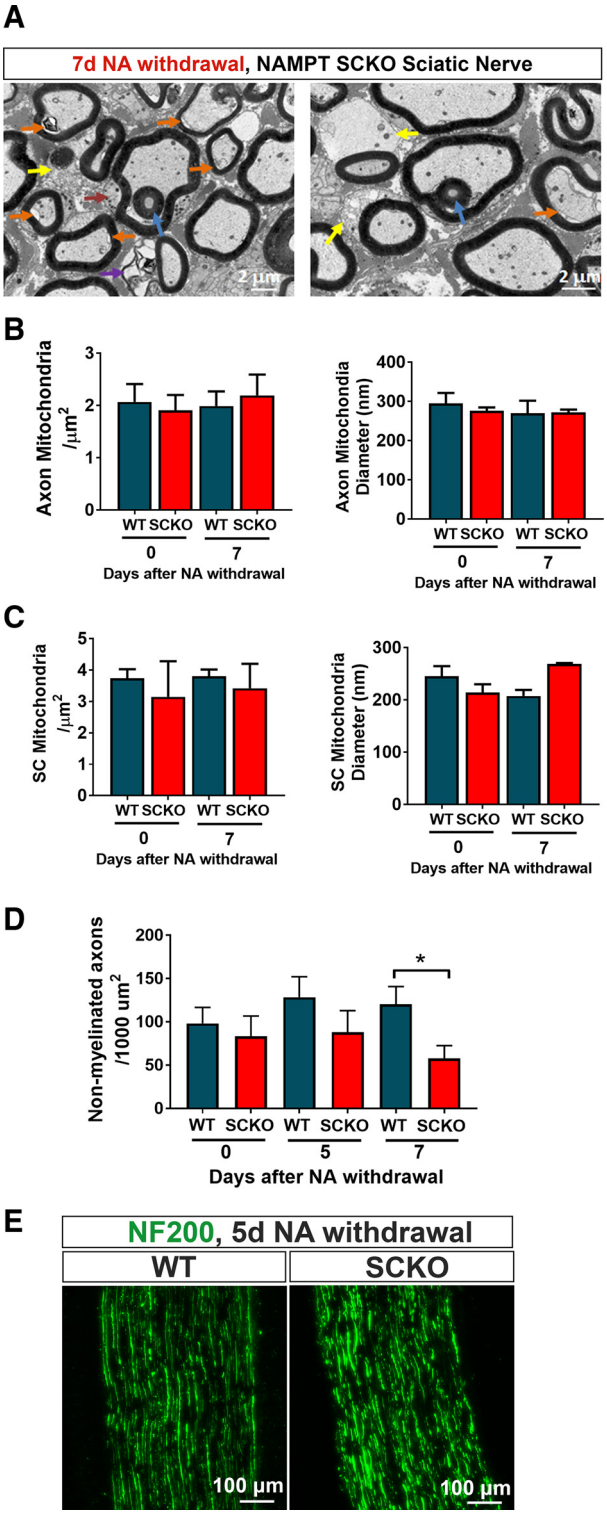

Figure 7. NA withdrawal leads to myelin degeneration. ***A***, Electron microscopic images of aberrant axons in NAMPT SCKO mice after NA withdrawal. Blue arrow indicates infolding. Purple arrow indicates interlamellar myelin splitting. Orange arrow indicates abnormal axo-glial junctions. Yellow arrow indicates abnormal SC cytoplasm at the outer tongue. Red arrow indicates an increased number of mitochondria within the SC cytoplasm. Mitochondria density and diameter were measured for axons (***B***) and SCs (***C***) at 0 and 7 d after NA depletion in WT and NAMPT SCKO sciatic nerves using EM images. ***D***, The density of nonmyelinated axons was determined at 0, 5, and 7 d after NA withdrawal in WT and NAMPT SCKO sciatic nerve EM images. *$p = 0.05$ (between brackets using unpaired two-tailed Student's *t* test). ***E***, Immunostaining of axons (NF200, green) in WT and NAMPT SCKO sciatic nerves at 5 d after NA withdrawal. Data are mean ± SEM. $n = 3$ or 4 mice for all experiments.

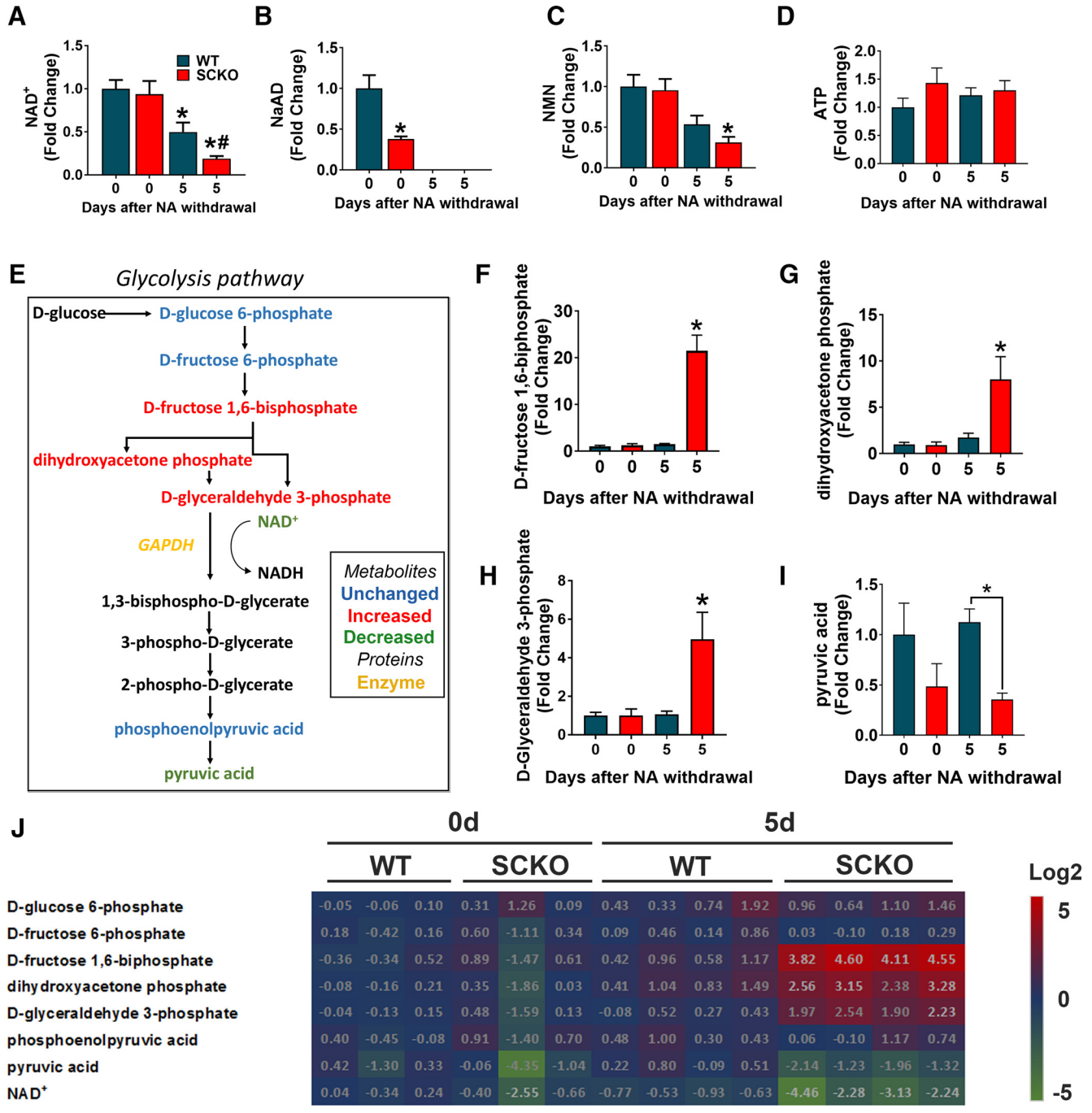

Figure 8. NA administration rescues NAD $^+$ deficiency in NAMPT SCKO nerves, and withdrawal leads to changes in glycolysis and the pentose phosphate pathway. ***A–D***, The metabolite levels of NAD $^+$ (***A***), NaAD (***B***), NMN (***C***), and ATP (***D***) at 0 and 5 d after NA withdrawal in P60 WT and NAMPT SCKO sciatic nerves treated with NA were determined by LC-MS/MS. Metabolite levels were normalized by the protein content in each sample and expressed relative to WT 0 d after NA withdrawal. ***A***, One-way ANOVA ($F_{(3,11)} = 12.4, p = 0.0007$). *$p < 0.03$, compared with WT with no NA withdrawal. #$p = 0.0033$, compared with NAMPT SCKO with no NA withdrawal ($n = 3–5$) with multiple comparisons with Sidak's *post hoc* test. ***B***, One-way ANOVA ($F_{(3,11)} = 49.79, p < 0.0001$). *$p = 0.004$, compared with WT with no NA withdrawal with multiple comparisons with Sidak's *post hoc* test ($n = 3–5$). ***C***, One-way ANOVA ($F_{(3,11)} = 8.049, p = 0.0041$). *$p < 0.02$, compared with WT or NAMPT SCKO with no NA withdrawal ($n = 3–5$). ***D***, One-way ANOVA ($F_{(3,11)} = 0.8632, p = 0.4889$), no significant difference ($n = 3–5$). ***E***, The glycolysis pathway. Black represents metabolites that were not detected. Blue represents metabolites that were detected but not significantly changed. Green represents metabolites that were significantly downregulated. Red represents metabolites that were significantly upregulated in NAMPT SCKO sciatic nerves at 5 d after NA withdrawal (relative to WT 0 d after NA withdrawal). Legend shown at the bottom right corner. ***F–J***, Ion abundance of each metabolites were normalized to the protein content and expressed relative to WT 0 d after NA withdrawal. The glycolysis intermediates (***F***) D-fructose 1,6-biphosphate, (***G***) dihydroxyacetone phosphate, and (***H***) D-glyceraldehyde 3-phosphate were all significantly upregulated in NAMPT SCKO sciatic nerves 5 d after NA withdrawal. ***I***, Pyruvic acid is significantly decreased in WT versus SCKO nerves 5 d after NA withdrawal. ***F***, One-way ANOVA ($F_{(3,10)} = 28.55, p < 0.0001$). *$p < 0.0001$, compared with all other groups with multiple comparisons with Sidak's *post hoc* test ($n = 3–5$). ***G***, One-way ANOVA ($F_{(3,10)} = 23.19, p < 0.0001$). *$p = 0.0004$ ($n = 3–5$) compared with all other groups with multiple comparisons with Sidak's *post hoc* test. ***H***, One-way ANOVA ($F_{(3,10)} = 23.54, p < 0.0001$). *$p = 0.0004$ ($n = 3–5$) compared with all other groups with multiple comparisons with Sidak's *post hoc* test. ***I***, *$p = 0.03$ ($n = 3–5$) compared between brackets with unpaired two-tailed Student's *t* test. ***J***, Heat map displaying levels of glycolysis metabolites and NAD $^+$ at 0 and 5 d after NA depletion. Each metabolite level was normalized to the average values of WT 0 d after NA withdrawal and $\log_2$ of fold changes are indicated by the number and color code. Data are mean ± SEM.

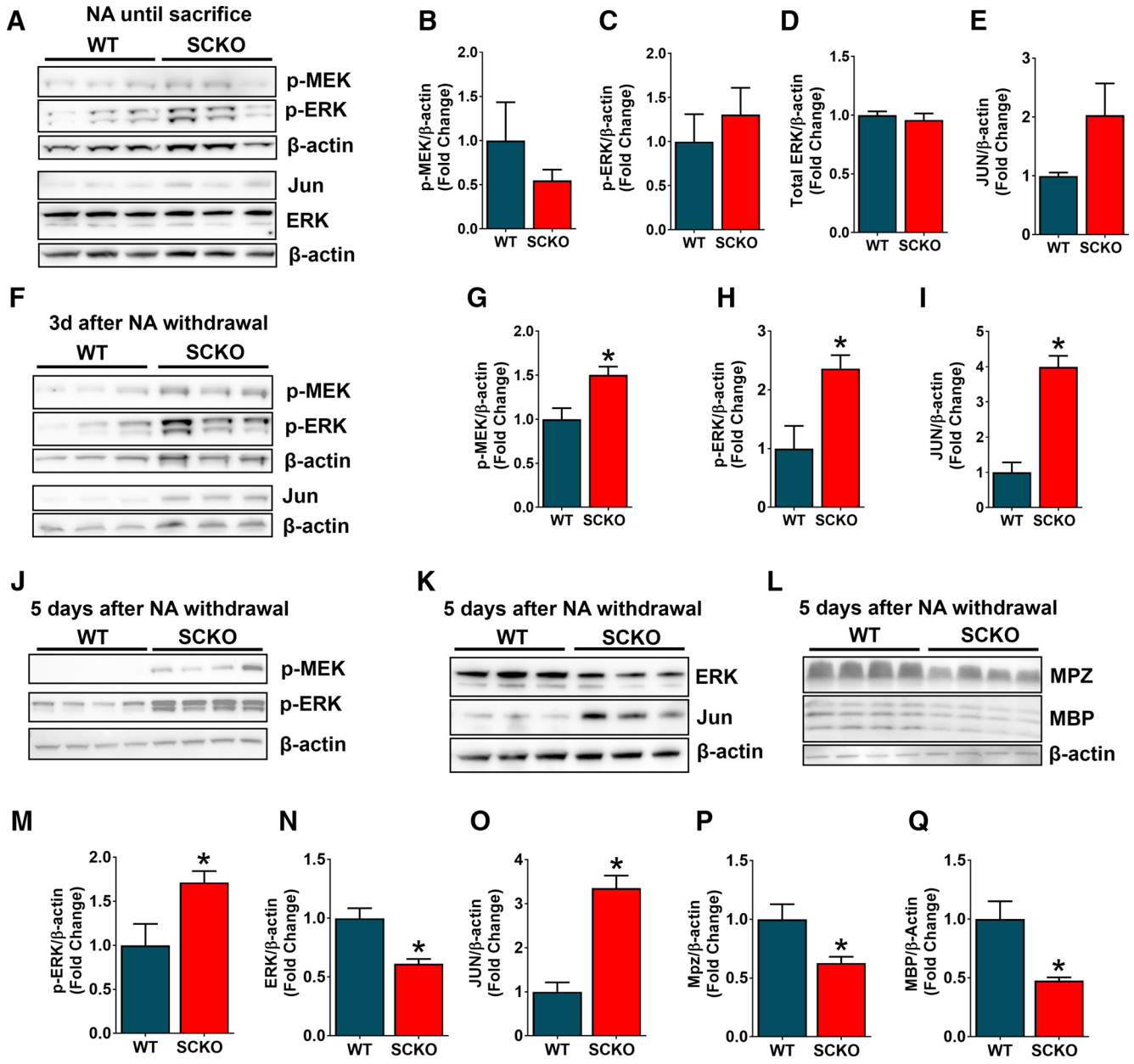

Figure 9. NA withdrawal leads to upregulation of SC dedifferentiation markers. ***A***, Western blot analysis of p-MEK, p-ERK, ERK, and JUN expression in sciatic nerves from WT and NAMPT SCKO treated with NA. ***B–E***, Quantification of protein expression levels from ***A*** normalized to β-actin for (***B***) p-MEK, (***C***) p-ERK, (***D***) total ERK, and (***E***) JUN. ***F***, Western blot analysis of p-MEK, p-ERK, and JUN expression in sciatic nerves from WT and NAMPT SCKO that were treated with NA until P55, then received normal drinking water for (***F***) 3 d or (***J–L***) 5 d. ***G–I***, Quantifications of the protein expression levels normalized to β-actin for (***G***) p-MEK, (***H***) p-ERK, and (***I***) JUN from ***F***, ***M***, p-ERK from ***J***, ***N***, total ERK, and (***O***) JUN from ***K***, ***P***, MPZ from ***Q***, and MBP from ***L***. ***B–E***, ***G–I***, ***M–Q***, Student's two-tailed *t* test $n = 3$ mice. ***G***, $^*p = 0.03$. ***H***, ***M***, $^*p = 0.04$. ***I***, $^*p = 0.002$. ***N***, $^*p = 0.02$. ***O***, $^*p = 0.003$. ***Q***, $^*p = 0.01$. Data are mean ± SEM.

show normal nerve morphology and function when treated with NA. However, when NA is withdrawn, nerve conduction is severely and rapidly decreased concomitant with aberrant myelination and inhibition of glycolysis. The MEK/ERK/JUN signaling cascade is activated soon after NA depletion, supporting the idea that aberrant SC dedifferentiation underlies these abnormalities. The rapid demyelination observed in this regulable neuropathy model provides a unique opportunity to study the early phase of the demyelination process. Overall, our results suggest that deregulation of NAD$^+$ homeostasis is a potential risk factor for demyelinating peripheral neuropathy through aberrant activation of the SC dedifferentiation program.

NAMPT SCKO mice show severe NAD$^+$ reduction, yet SC viability is unchanged, suggesting the existence of SC compensatory mechanisms that prevent cell death despite metabolic challenges. In contrast to SC viability, SC differentiation and myelination are strongly dependent on metabolic status (Rangaraju et al., 2009; Fünfschilling et al., 2012; Viader et al., 2013; Beirowski et al., 2014; Norrmén et al., 2014). Our metabolomics analysis revealed a reduction of GAPDH activity in NAMPT SCKO nerves, which resulted in decreased pyruvate levels. Although pyruvate is a precursor of acetyl CoA, an important component of energy production via the TCA cycle, ATP levels were maintained in NAMPT-SCKO nerves. This suggests a compensatory metabolic adaptation to maintain essential energetics, perhaps by shunting acetyl CoA away from the cytosol for use in fatty acid synthesis and using it preferentially in the mitochondria for energy production. Such a metabolic shift would result in re-

duced lipid production and presumably a deficit in myelin formation and/or maintenance. Indeed, SC-specific loss of the metabolic regulator LKB1 results in severe peripheral neuropathy due to the loss of citrate, the precursor for cytosolic acetyl CoA, and a reduction in major myelin lipid classes (Pooya et al., 2014). These results suggest that hypomyelination in NAMPT SCKO mice could result from compensatory pathways that maintain viability but result in reduced fatty acid production.

NAMPT SCKO mice show severe delay of SC maturation together with altered expression of SC differentiation genes. NAD^+ metabolism could affect expression of SC differentiation genes through regulation of sirtuin-dependent protein acetylation or directly by altered synthesis of the acetylation substrate, acetyl CoA. SIRT1 deacetylates and destabilizes NOTCH, an important regulator of SC differentiation and myelination (Woodhoo et al., 2009; Guarani et al., 2011). In another example, SC myelination is dependent on NF-κB p65, whose activity is regulated by deacetylation mediated by HDAC1/2 (Chen et al., 2011). Radial sorting and myelination are influenced by the recruitment of the histone acetyltransferase p300 to selected enhancers by the SWI/SNF family of chromatin-remodeling complexes (Weider et al., 2012; Alver et al., 2017). Overall, these results suggest that NAD^+ metabolism causes epigenetic changes that alter genetic networks leading to abnormalities in SC differentiation/dedifferentiation pathways.

In addition to the above transcriptional changes, we found a significant increase in MEK/ERK/JUN signaling at 3 d after NA depletion in NAMPT SCKO nerves. Activation of this pathway is observed in dedifferentiating SCs after nerve injury (Arthur-Farraj et al., 2012) and is sufficient to drive SC dedifferentiation in adult nerves (Napoli et al., 2012; Fazal et al., 2017). It is well known that sciatic nerve transection initiates a rapid decline in NAD^+ in the distal portion of the nerve (Gerdts et al., 2015; Sasaki et al., 2016); however, whether this occurs in SCs or only in the axonal component is unknown. The activation of ERK/MEK/JUN signaling upon NAD^+ reduction in the absence of nerve injury suggests that the SC dedifferentiation observed after injury could be induced by changes in NAD^+ homeostasis.

Upon NA withdrawal, the nerves in adult NAMPT SCKO mice underwent a rapid disruption of the interaction between SCs and axons, as well as the breakdown of myelin structures characterized by interlamellar splitting of myelin sheath. The disruption of SC-axon contacts is essential for the insulation and SC-mediated trophic support of axons and is one of the earliest signs of demyelinating neuropathy (de Waegh et al., 1992; Yin et al., 1998). The detachment of the SC myelin sheath from the axon has also been observed in mutant mice lacking either the cell adhesion molecule CADM4 or the tight junction protein CLDN19 (Miyamoto et al., 2005; Golan et al., 2013), both of which develop severe peripheral neuropathy. How NAD^+ levels might regulate SC-axon adhesion, either through these proteins or others, will require additional investigation.

NA administration restored NAD^+ levels and rescued most abnormalities found in NAMPT SCKO mice, including shortened life span, hypomyelination, electrophysiological defects, and abnormal activation of SC dedifferentiation signals. However, NA administration did not completely rescue all SC defects. This is evidenced by the continued absence of SC cytoplasm that divides small-fiber axons in Remak bundles, suggesting that the radial sorting deficits are incompletely reversed. This recalcitrant defect could reflect differences in NAD^+ metabolism in nonmyelinating SCs. For instance, their ability to produce NAD^+ from NA may be restricted due to low levels of NAPRT and/or NAD^+ synthetase. If this is the case, future experiments aimed at rescuing Remak axonal sorting by an alternative route of NMN supply may provide further insights. The absence of SC cytoplasm between Remak bundle axons is also found in mice with SC-specific mutations in other metabolic proteins, including TFAM (Viader et al., 2011), COX10 (Fünfschilling et al., 2012), and LKB1 (Beirowski et al., 2014). In addition, LRP1, low-density lipoprotein receptor family protein (Orita et al., 2013), and BRG1, a core protein in the BAF chromatin remodeling complex, are also required for Remak axonal sorting (Weider et al., 2012). It will be important to determine whether NAD^+ levels influence the function or expression of these regulators, as the sensory fibers affected by these abnormalities are a central target of many peripheral neuropathies, including those caused by diabetes and aging.

NAMPT-mediated NAD^+ synthesis is chronically impaired in various tissues in aged or Type 2 diabetic mice (Yoshino et al., 2011; Stein and Imai, 2014; Verdin, 2015). In addition, the primary enzyme mediating NAD^+ degradation, CD38, increases with age. The impact of chronic lower levels of NAD^+ in the peripheral nervous system is not well studied, but it likely contributes to the association of neuropathy with increasing age and metabolic syndromes (Feldman et al., 2017). Our current findings reveal crucial roles of NAD^+ homeostasis in peripheral nerve maintenance. In particular, the need for adequate NAD^+ levels in suppressing SC dedifferentiation in adult nerve provides new insights that may lead to alternative approaches for treating peripheral neuropathies.

References

Alver BH, Kim KH, Lu P, Wang X, Manchester HE, Wang W, Haswell JR, Park PJ, Roberts CW (2017) The SWI/SNF chromatin remodelling complex is required for maintenance of lineage specific enhancers. Nat Commun 8:14648. CrossRef Medline

Arthur-Farraj PJ, Latouche M, Wilton DK, Quintes S, Chabrol E, Banerjee A, Woodhoo A, Jenkins B, Rahman M, Turmaine M, Wicher GK, Mitter R, Greensmith L, Behrens A, Raivich G, Mirsky R, Jessen KR (2012) c-Jun reprograms Schwann cells of injured nerves to generate a repair cell essential for regeneration. Neuron 75:633–647. CrossRef Medline

Bacallao K, Monje PV (2015) Requirement of cAMP signaling for Schwann cell differentiation restricts the onset of myelination. PLoS One 10: e0116948. CrossRef Medline

Beirowski B, Gustin J, Armour SM, Yamamoto H, Viader A, North BJ, Michán S, Baloh RH, Golden JP, Schmidt RE, Sinclair DA, Auwerx J, Milbrandt J (2011) Sir-two-homolog 2 (Sirt2) modulates peripheral myelination through polarity protein par-3/atypical protein kinase C (aPKC) signaling. Proc Natl Acad Sci U S A 108:E952–E961. CrossRef Medline

Beirowski B, Babetto E, Golden JP, Chen YJ, Yang K, Gross RW, Patti GJ, Milbrandt J (2014) Metabolic regulator LKB1 is crucial for Schwann cell-mediated axon maintenance. Nat Neurosci 17:1351–1361. CrossRef Medline

Cervellini I, Galino J, Zhu N, Allen S, Birchmeier C, Bennett DL (2018) Sustained MAPK/ERK activation in adult Schwann cells impairs nerve repair. J Neurosci 38:679–690. CrossRef Medline

Chan KY, Jang MJ, Yoo BB, Greenbaum A, Ravi N, Wu WL, Sánchez-Guardado L, Lois C, Mazmanian SK, Deverman BE, Gradinaru V (2017) Engineered AAVs for efficient noninvasive gene delivery to the central and peripheral nervous systems. Nat Neurosci 20:1172–1179. CrossRef Medline

Chen Y, Wang H, Yoon SO, Xu X, Hottiger MO, Svaren J, Nave KA, Kim HA, Olson EN, Lu QR (2011) HDAC-mediated deacetylation of NF-κB is critical for Schwann cell myelination. Nat Neurosci 14:437–441. CrossRef Medline

de Waegh SM, Lee VM, Brady ST (1992) Local modulation of neurofilament phosphorylation, axonal caliber, and slow axonal transport by myelinating Schwann cells. Cell 68:451–463. CrossRef Medline

Fazal SV, Gomez-Sanchez JA, Wagstaff LJ, Musner N, Otto G, Janz M, Mirsky

R, Jessen KR (2017) Graded elevation of c-Jun in Schwann cells in vivo: gene dosage determines effects on development, re-myelination, tumorigenesis and hypomyelination. J Neurosci 37:12297–12313. CrossRef Medline

Feldman EL, Nave KA, Jensen TS, Bennett DLH (2017) New horizons in diabetic neuropathy: mechanisms, bioenergetics, and pain. Neuron 93: 1296–1313. CrossRef Medline

Feltri ML, D'Antonio M, Previtali S, Fasolini M, Messing A, Wrabetz L (1999) P0-cre transgenic mice for inactivation of adhesion molecules in Schwann cells. Ann N Y Acad Sci 883:116–123. CrossRef Medline

Feltri ML, Poitelon Y, Previtali SC (2015) How Schwann cells sort axons new concepts. Neuroscientist 1:1–14. CrossRef Medline

Frederick DW, Loro E, Liu L, Davila A Jr, Chellappa K, Silverman IM, Quinn WJ 3rd, Gosai SJ, Tichy ED, Davis JG, Mourkioti F, Gregory BD, Dellinger RW, Redpath P, Migaud ME, Nakamaru-Ogiso E, Rabinowitz JD, Khurana TS, Baur JA (2016) Loss of NAD homeostasis leads to progressive and reversible degeneration of skeletal muscle. Cell Metab 24:269–282. CrossRef Medline

Fünfschilling U, Supplie LM, Mahad D, Boretius S, Saab AS, Edgar J, Brinkmann BG, Kassmann CM, Tzvetanova ID, Möbius W, Diaz F, Meijer D, Suter U, Hamprecht B, Sereda MW, Moraes CT, Frahm J, Goebbels S, Nave KA (2012) A glycolytic oligodendrocytes maintain myelin and long-term axonal integrity. Nature 485:517–521. CrossRef Medline

Gavrieli Y, Sherman Y, Ben-Sasson SA (1992) Identification of programmed cell death in situ via specific labeling of nuclear DNA fragmentation. J Cell Biol 119:493–501. CrossRef Medline

Geisler S, Doan RA, Strickland A, Huang X, Milbrandt J, DiAntonio A (2016) Prevention of vincristine-induced peripheral neuropathy by genetic deletion of SARM1 in mice. Brain 139:3092–3108. CrossRef Medline

Gerdts J, Brace EJ, Sasaki Y, DiAntonio A, Milbrandt J (2015) SARM1 activation triggers axon degeneration locally via NAD$^+$ destruction. Science 348:453–457. CrossRef Medline

Golan N, Kartvelishvily E, Spiegel I, Salomon D, Sabanay H, Rechav K, Vainshtein A, Frechter S, Maik-Rachline G, Eshed-Eisenbach Y, Momoi T, Peles E (2013) Genetic deletion of Cadm4 results in myelin abnormalities resembling Charcot-Marie-Tooth neuropathy. J Neurosci 33:10950–10961. CrossRef Medline

Guarani V, Deflorian G, Franco CA, Krüger M, Phng LK, Bentley K, Toussaint L, Dequiedt F, Mostoslavsky R, Schmidt MH, Zimmermann B, Brandes RP, Mione M, Westphal CH, Braun T, Zeiher AM, Gerhardt H, Dimmeler S, Potente M (2011) Acetylation-dependent regulation of endothelial notch signalling by the SIRT1 deacetylase. Nature 473:234–238. CrossRef Medline

Hackett AR, Lee DH, Dawood A, Rodriguez M, Funk L, Tsoulfas P, Lee JK (2016) STAT3 and SOCS3 regulate NG2 cell proliferation and differentiation after contusive spinal cord injury. Neurobiol Dis 89:10–22. CrossRef Medline

Hasmann M, Schemainda I (2003) FK866, a highly specific noncompetitive inhibitor of nicotinamide phosphoribosyltransferase, represents a novel mechanism for induction of tumor cell apoptosis. Cancer Res 63:7436–7442. Medline

Imai S, Guarente L (2014) NAD$^+$ and sirtuins in aging and disease. Trends Cell Biol 24:464–471. CrossRef Medline

Jessen KR, Mirsky R (2005) The origin and development of glial cells in peripheral nerves. Nat Rev Neurosci 6:671–682. CrossRef Medline

Kim S, Maynard JC, Sasaki Y, Strickland A, Sherman DL, Brophy PJ, Burlingame AL, Milbrandt J (2016) Schwann cell O-GlcNAc glycosylation is required for myelin maintenance and axon integrity. J Neurosci 36:9633–9646. CrossRef Medline

Lin JB, Kubota S, Ban N, Yoshida M, Santeford A, Sene A, Nakamura R, Zapata N, Kubota M, Tsubota K, Yoshino J, Imai SI, Apte RS (2016) NAMPT-mediated NAD$^+$ biosynthesis is essential for vision in mice. Cell Rep 17:69–85. CrossRef Medline

Lukasova M, Malaval C, Gille A, Kero J, Offermanns S (2011) Nicotinic acid inhibits progression of atherosclerosis in mice through its receptor GPR109A expressed by immune cells. J Clin Invest 121:1163–1173. CrossRef Medline

Miyamoto T, Morita K, Takemoto D, Takeuchi K, Kitano Y, Miyakawa T, Nakayama K, Okamura Y, Sasaki H, Miyachi Y, Furuse M, Tsukita S (2005) Tight junctions in Schwann cells of peripheral myelinated axons: a lesson from claudin-19-deficient mice. J Cell Biol 169:527–538. CrossRef Medline

Nagarajan R, Svaren J, Le N, Araki T, Watson M, Milbrandt J (2001) EGR2 mutations in inherited neuropathies dominant-negatively inhibit myelin gene expression. Neuron 30:355–368. Medline

Napoli I, Noon LA, Ribeiro S, Kerai AP, Parrinello S, Rosenberg LH, Collins MJ, Harrisingh MC, White IJ, Woodhoo A, Lloyd AC (2012) A central role for the ERK-signaling pathway in controlling Schwann cell plasticity and peripheral nerve regeneration in vivo. Neuron 73:729–742. CrossRef Medline

Nave KA (2010) Myelination and support of axonal integrity by glia. Nature 468:244–252. CrossRef Medline

Nikiforov A, Kulikova V, Ziegler M (2015) The human NAD metabolome: functions, metabolism and compartmentalization. Crit Rev Biochem Mol Biol 50:284–297. CrossRef Medline

Norrmén C, Figlia G, Lebrun-Julien F, Pereira JA, Trötzmüller M, Köfeler HC, Rantanen V, Wessig C, van Deijk AL, Smit AB, Verheijen MH, Rüegg MA, Hall MN, Suter U (2014) mTORC1 controls PNS myelination along the mTORC1-RXRγ-SREBP-lipid biosynthesis axis in Schwann cells. Cell Rep 9:646–660. CrossRef Medline

Orita S, Henry K, Mantuano E, Yamauchi K, De Corato A, Ishikawa T, Feltri ML, Wrabetz L, Gaultier A, Pollack M, Ellisman M, Takahashi K, Gonias SL, Campana WM (2013) Schwann cell LRP1 regulates remak bundle ultrastructure and axonal interactions to prevent neuropathic pain. J Neurosci 33:5590–5602. CrossRef Medline

Parkinson DB, Bhaskaran A, Arthur-Farraj P, Noon LA, Woodhoo A, Lloyd AC, Feltri ML, Wrabetz L, Behrens A, Mirsky R, Jessen KR (2008) c-jun is a negative regulator of myelination. J Cell Biol 181:625–637. CrossRef Medline

Pooya S, Liu X, Kumar VB, Anderson J, Imai F, Zhang W, Ciraolo G, Ratner N, Setchell KD, Yoshida Y,Yutaka Y, Jankowski MP, Dasgupta B, Dasgupta B (2014) The tumour suppressor LKB1 regulates myelination through mitochondrial metabolism. Nat Commun 5:4993. CrossRef Medline

Rangaraju S, Hankins D, Madorsky I, Madorsky E, Lee WH, Carter CS, Leeuwenburgh C, Notterpek L (2009) Molecular architecture of myelinated peripheral nerves is supported by calorie restriction with aging. Aging Cell 8:178–191. CrossRef Medline

Ratner N, Williams JP, Kordich JJ, Kim HA (2006) Schwann cell preparation from single mouse embryos: analyses of neurofibromin function in Schwann cells. Methods Enzymol 407:22–33. CrossRef Medline

Rongvaux A, Galli M, Denanglaire S, Van Gool F, Drèze PL, Szpirer C, Bureau F, Andris F, Leo O (2008) Nicotinamide phosphoribosyl transferase/pre-B cell colony-enhancing factor/visfatin is required for lymphocyte development and cellular resistance to genotoxic stress. J Immunol 181: 4685–4695. CrossRef Medline

Salzer JL (2008) Switching myelination on and off. J Cell Biol 181:575–577. CrossRef Medline

Salzer JL (2015) Schwann cell myelination. Cold Spring Harb Perspect Biol 7:a020529. CrossRef Medline

Sasaki Y, Nakagawa T, Mao X, DiAntonio A, Milbrandt J (2016) NMNAT1 inhibits axon degeneration via blockade of SARM1-mediated NAD(+) depletion. Elife 5:e19749. CrossRef Medline

Stein LR, Imai S (2014) Specific ablation of Nampt in adult neural stem cells recapitulates their functional defects during aging. EMBO J 33:1321–1340. CrossRef Medline

Stein LR, Wozniak DF, Dearborn JT, Kubota S, Apte RS, Izumi Y, Zorumski CF, Imai S (2014) Expression of Nampt in hippocampal and cortical excitatory neurons is critical for cognitive function. J Neurosci 34:5800–5815. CrossRef Medline

Stromsdorfer KL, Yamaguchi S, Yoon MJ, Moseley AC, Franczyk MP, Kelly SC, Qi N, Imai S, Yoshino J (2016) NAMPT-mediated NAD$^+$ biosynthesis in adipocytes regulates adipose tissue function and multi-organ insulin sensitivity in mice. Cell Rep 16:1851–1860. CrossRef Medline

Tan B, Dong S, Shepard RL, Kays L, Roth KD, Geeganage S, Kuo MS, Zhao G (2015) Inhibition of nicotinamide phosphoribosyltransferase (NAMPT), an enzyme essential for NAD$^+$ biosynthesis, leads to altered carbohydrate metabolism in cancer cells. J Biol Chem 290:15812–15824. CrossRef Medline

Tolstikov V, Nikolayev A, Dong S, Zhao G, Kuo MS (2014) Metabolomics analysis of metabolic effects of nicotinamide phosphoribosyltransferase (NAMPT) inhibition on human cancer cells. PLoS One 9:e114019. CrossRef Medline

Verdin E (2015) NAD+ in aging, metabolism, and neurodegeneration. Science 350:1208–1213. CrossRef Medline

Viader A, Golden JP, Baloh RH, Schmidt RE, Hunter DA, Milbrandt J (2011) Schwann cell mitochondrial metabolism supports long-term axonal survival and peripheral nerve function. J Neurosci 31:10128–10140. CrossRef Medline

Viader A, Sasaki Y, Kim S, Strickland A, Workman CS, Yang K, Gross RW, Milbrandt J (2013) Aberrant Schwann cell lipid metabolism linked to mitochondrial deficits leads to axon degeneration and neuropathy. Neuron 77:886–898. CrossRef Medline

Weider M, Küspert M, Bischof M, Vogl MR, Hornig J, Loy K, Kosian T, Müller J, Hillgärtner S, Tamm ER, Metzger D, Wegner M (2012) Chromatin-remodeling factor Brg1 is required for Schwann cell differentiation and myelination. Dev Cell 23:193–201. CrossRef Medline

Woodhoo A, Alonso MB, Droggiti A, Turmaine M, D'Antonio M, Parkinson DB, Wilton DK, Al-Shawi R, Simons P, Shen J, Guillemot F, Radtke F, Meijer D, Feltri ML, Wrabetz L, Mirsky R, Jessen KR (2009) Notch controls embryonic Schwann cell differentiation, postnatal myelination and adult plasticity. Nat Neurosci 12:839–847. CrossRef Medline

Yin X, Crawford TO, Griffin JW, Tu P, Lee VM, Li C, Roder J, Trapp BD (1998) Myelin-associated glycoprotein is a myelin signal that modulates the caliber of myelinated axons. J Neurosci 18:1953–1962. CrossRef Medline

Yoshino J, Mills KF, Yoon MJ, Imai S (2011) Nicotinamide mononucleotide, a key NAD+ intermediate, treats the pathophysiology of diet- and age-induced diabetes in mice. Cell Metab 14:528–536. CrossRef Medline

Zhang LQ, Van Haandel L, Xiong M, Huang P, Heruth DP, Bi C, Gaedigk R, Jiang X, Li DY, Wyckoff G, Grigoryev DN, Gao L, Li L, Wu M, Leeder JS, Ye SQ (2017) Metabolic and molecular insights into an essential role of nicotinamide phosphoribosyltransferase. Cell Death Dis 8:e2705. CrossRef Medline